EXPERIMENTAL INVESTIGATION OF DETACHED SHOCK ON A 70° CONE AT VARIOUS ANGLES OF ATTACK

Thesis by

William C. Bryan, LCdr., U. S. Navy

In Partial Fulfillment of the Requirements

For the Degree of

Aeronautical Engineer

California Institute of Technology

Pasadena, California

1950

ACKNOWLEDGEMENTS

This investigation was conducted jointly with LCdr. Leo F. Frick, U. S. Navy. The author desires to express his appreciation to Dr. Henry T. Nagamatsu for his advice and assistance in the conduct of this investigation.

ABSTRACT

The results of an experimental investigation into the variation of the shock wave shape and the extent of the subsonic region behind the shock with varying angle of attack at various Mach numbers are summarized. All tests are made on a finite 70° cone. The main interest is centered on those Mach numbers which are low enough to produce detached shocks or for which the possibility of detachment exists for increasing angles of attack.

The angles of attack for which the investigation is made are 0°, 3°, 6°, 9°, 12°, and 15°. The Mach numbers considered are 1.438, 1.544, 1.584, 1.857, 1.986, and 3.01.

It is found that, for increasing angles of attack at constant Mach numbers, the extent of the subsonic region increases behind the lower shock and decreases behind the upper shock. A subsonic region appears at increased angle of attack for two of the Mach numbers for which the shocks are initially attached. There is also quite definite interaction between the upper and lower portions of the shock which tends to inhibit both the appearance of a subsonic region after the shock on the one hand and the disappearance of it on the other.

TABLE OF CONTENTS

Part	Title	Page
	Acknowledgements	i
	Abstract	ii
	Table of Contents	iii
	List of Figures	iv
	List of Tables	vi
I.	Introduction	1
II.	Equipment and Procedure	2
III.	Results and Discussion	5
IV.	Conclusions	10
	References	11
	Sample Calculations	12
	Tables	14
	Figures	28

LIST OF FIGURES

Figure No.	Title	Page
1	Pressure Orifice Location on Models	28
2	Symbols	29
3	Shock Wave Pattern, M = 1.438, Lower	30
4	Shock Wave Pattern, M = 1.438, Upper	31
5	Shock Wave Pattern, M = 1.544, Lower	32
6	Shock Wave Pattern, M = 1.544, Upper	33
7	Shock Wave Pattern, M = 1.584, Lower	34
8	Shock Wave Pattern, M = 1.584, Upper	35
9	Shock Wave Pattern, M = 1.857, Lower	36
10	Shock Wave Pattern, M = 1.857, Upper	37
11	Shock Wave Pattern, M = 1.986, Lower	38
12	Shock Wave Pattern, M = 1.986, Upper	39
13	Shock Wave Pattern, M = 3.01, Lower	40
14	Shock Wave Pattern, M = 3.01, Upper	41
15	Shock Wave Pattern, $\alpha = 0^{\circ}$, Upper and Lower	42
16	Shock Wave Pattern, $\alpha = 3^{\circ}$, Lower	43
17	Shock Wave Pattern, $\alpha = 3^{\circ}$, Upper	44
18	Shock Wave Pattern, $\alpha = 6^{\circ}$, Lower	45
19	Shock Wave Pattern, $\alpha = 6^{\circ}$, Upper	46

LIST OF FIGURES (continued)

Figure No.	Title	Page
20	Shock Wave Pattern, $\alpha = 9^{\circ}$, Lower	47
21	Shock Wave Pattern, $\alpha = 9^{\circ}$, Upper	48
22	Shock Wave Pattern, $\alpha = 12^{\circ}$, Lower	49
23	Shock Wave Pattern, $\alpha = 12^{\circ}$, Upper	50
24	Shock Wave Pattern, $\alpha = 15^{\circ}$, Lower	51
25	Shock Wave Pattern, $\alpha = 15^{\circ}$, Upper	52
26	Maximum Flow Deflection (Taylor-Maccoll Theory)	53
27	Surface Pressure Distribution, $M = 1.584$	54
28	Schlieren Picture, $M = 1.544$, $\alpha = 0^{\circ}$	55
29	Schlieren Picture, $M = 1.544$, $\alpha = 15^{\circ}$	55
30	Schlieren Picture, $M = 1.584$, $\alpha = 0^{\circ}$	56
31	Schlieren Picture, $M = 1.584$, $\alpha = 15^{\circ}$	56
32	Schlieren Picture, $M = 1.857$, $\alpha = 0^{\circ}$	57
33	Schlieren Picture, $M = 1.857$, $\alpha = 15^{\circ}$	57

LIST OF TABLES

Table No.	Subject	Page
I.	Tabulation of Mach Number Behind Shock, M = 1.438	14
II.	Tabulation of Mach Number Behind Shock, M = 1.544	17
III.	Tabulation of Mach Number Behind Shock, M = 1.584	20
IV.	Tabulation of Mach Number Behind Shock, M = 1.857	23
V.	Tabulation of Mach Number Behind Shock, M = 1.986	25
VI.	Tabulation of Mach Number Behind Shock, M = 3.01	26
VII.	Condition of Shock	27

I. INTRODUCTION

The general objective of this investigation was the experimental determination of the shock wave shape and its allied characteristics due to the presence of a finite, 70° cone in a supersonic flow at various angles of attack. The main interest was to be centered on detached shocks and those attached shocks for which there was a possibility of detachment occurring as angle of attack was increased, and particular interest was to be given to the subsonic regime of flow behind the shock. Pressure measurements at the cone surface were not to be attempted extensively, but were desired only for one Mach number at zero angle of attack and at a relatively high angle of attack.

As far as is known, no previous experimental work has been done on detached shock variations with angle of attack for three-dimensional flow. B. W. Marschner, (Cf. Ref. 1), V. I. Muirhead, and Neil MacKinnon, (Cf. Ref. 2), have previously investigated detached shock wave shapes, Mach number behind the shock, and pressure distribution for similar cones throughout the same range of Mach numbers at zero angle of attack. This investigation was intended to carry their work one step further.

Since theoretical study of the detached shock phenomenon has not yet progressed to the point where a prediction of the behaviour of shock waves at various angle of attack can be made, this investigation, it was hoped, would furnish some small insight into this interesting phase of supersonics, and perhaps point the way to further study.

II. EQUIPMENT AND PROCEDURE

Six cone models were used for this investigation. The models were identical, 3/8" in diameter, and had a cone angle of 70°. Each model was equipped with a pressure orifice located on the conical surface at distances from the nose which varied from model to model. The dimensions of the cone model and the location of the pressure orifices are indicated in Fig. 1.

The investigation was carried out in the GALCIT 2.5" Supersonic Wind Tunnel, (Cf. Ref. 3). The model was mounted on a sting which could be moved in elevation through an angle of attack range from -3° to +15°. No azimuthal variation was possible. In order to produce Mach numbers of 1.438, 1.544 and 1.857 a flexible nozzle with adjustable jacks was used. This nozzle is fully described in Ref. 1. Steel nozzle blocks were available for Mach numbers of 1.584, 1.986 and 3.01. The nozzle shapes for the flexible nozzle were computed by Puckett's Method, (Cf. Ref. 4). Boundary layer corrections were applied using Puckett's approximate figure.

In order to calibrate the test section Mach number a static pressure survey was made along the nozzle centerline in conjunction with a reference static pressure taken at the test section wall. The centerline survey was accomplished with a section of I.D. 0.065" tubing fixed by means of two rigid supports at either end of the nozzle so that movement

was possible in an axial direction only. This tubing was equipped with a small static orifice. In order to eliminate the necessity for measuring small changes in low pressure along the test section centerline against a relatively high atmospheric pressure, the centerline static pressure was measured against the reference pressure at the wall. The reference pressure was, in turn, measured against atmospheric pressure. By subtracting the difference in wall and centerline pressures from the average wall pressure the centerline static pressure was obtained.

In calibrating the model angle of attack the following procedure was used. Pressure readings were taken at three angles of attack with the model orifice on the top. Pressure readings at the same three angles of attack were then taken with the orifice on the bottom. These pressure readings were plotted against angle of attack; thus, intersection of top and bottom curves gave the zero angle of attack position.

Throughout the tests the relative humidity of the tunnel was kept within a range of .02 to .04 percent by means of a silica-gel dryer in the tunnel circuit.

After calibration of the nozzle and angle of attack, photographs of the flow around the model were taken by means of schlieren apparatus with the model at angles of attack varying from 0° to 15° in 3° increments.

Finally, a pressure survey at the cone surface was made at a Mach number of 1.584 for angles of attack of 0° and 12°, (Cf. Fig. 27).

The dimensionless shock wave patterns were obtained by the following procedure. The negatives of the flow photographs were projected on graph paper by means of a photographic enlarger. The enlarger was adjusted so that the diameter of the model was equal to a Y/D of one on the selected scale, and the shock wave pattern was traced. This same procedure was followed in tracing all shock wave patterns. In order to minimize the error in the relative displacement of the shocks from the model from one angle of attack to the next, all shock patterns for each particular Mach number were traced on the same sheet of graph paper. This procedure was also followed for each particular angle of attack and varying Mach number. The final dimensionless plots were obtained directly from these tracings. It was hoped, by this means, to minimize, in so far as was possible, the errors which are inevitable in transcribing such curves to dimensionless coordinates.

III. RESULTS AND DISCUSSION

The results of this investigation are presented in three forms. The shock wave patterns are plotted first with Mach number constant and angle of attack varying, (Cf. Figs. 3 to 14). Secondly, they are plotted with angle of attack constant and Mach numbers varying, (Cf. Figs. 15 to 25). The above plots are relative to the cone axis rather than to the flow direction. Thirdly, the Mach number (M_2) directly behind the shock is tabulated for each Mach number and angle of attack, (Cf. Tables I to VI). This tabulation is carried out only for the subsonic portion of the flow. In addition to the above tabulation, the point at which the Mach number behind the shock becomes sonic and the position of the normal shock are indicated on the shock wave plots. For Mach numbers of 1.857 and 1.986 the sonic points have not been indicated, to avoid confusion. These points are, however, indicated on the cross-plots of constant angle of attack.

A pressure survey on the surface of the cone at a Mach number of 1.584 was taken at 0° and 12° angles of attack for both upper and lower surfaces of the cone, (Cf. Fig. 27).

Symbols used in graphical and tabular presentation of the data are defined in Fig. 2.

The shock wave patterns were plotted in dimensionless form using the diameter of the cone as the characteristic dimension. Special care

was taken in obtaining the shape of the shock wave patterns near the nose of the cone since it was found that some of the shocks crossed in this region.

The shock wave patterns for constant Mach number show that close to the nose of the cone, the spread of the shocks is rather irregular with some crossing over others in an unpredictable manner; the spread, however, becomes regular with angle of attack as the distance from the nose along the shock increases. This is particularly true of the lower portions of the shock waves. As the angle of attack increases, the shocks associated with the upper surface of the cone tend to become straight and to assume the characteristics of an attached shock. Conversely, the lower portion of these shocks become more curved and thus more nearly assume detached characteristics. This is more clearly brought out by the Mach number survey directly behind the shock.

The variations in the shock wave pattern due to changing Mach number are plotted for each angle of attack, and are essentially a cross-plot of the previously discussed curves. These plots clearly show that, while the lower portions of the shocks gradually assume the curved configuration associated with detached shocks as the angle of attack increases, those shocks which were initially physically attached to the nose of the cone apparently remain attached for the angles of attack investigated. Conversely, shocks initially physically detached remain detached.

The Mach number directly behind the shock at each point under consideration was calculated by measuring the slope of the shock at that point relative to the flow direction. Two-dimensional oblique shock theory then gave the Mach number behind the shock, (Cf. Tables I to VI).

At an angle of attack of 0°, the subsonic region behind the shock is symmetrical with respect to the cone axis. As the angle of attack increases for each Mach number, the extent of the subsonic region increases behind the lower portion of the shock and decreases behind the upper portion. The rate of decrease, however, is considerably faster than the rate of increase. The overall effect is to decrease the total extent of the subsonic region as the angle of attack is increased. This effect is more pronounced for the lower Mach numbers. As the Mach number increases at each angle of attack the extent of the subsonic zone decreases in both the lower and upper portions of the flow.

If the assumption is made that the cone upper and lower surfaces can be considered separately and that the angle between the flow direction and the cone surface can be considered as the half-vertex angle of a fictitious cone, some comparison can be made with the Taylor-Maccoll theory for conical shocks, (Cf. Ref. 5). Fig. 26 was prepared to illustrate the maximum flow deflection for a given initial Mach number using this theory. Table VII indicates the condition of

shock for each Mach number for both upper and lower shocks.

First considering the lower shocks at zero angle of attack, the shock has detached characteristics until a Mach number between 1.584 and 1.857 is reached, where it assumes attached characteristics. This is in agreement with the Taylor-Maccoll theory. The results also agree for 3°. At an angle of attack of 6°, which corresponds to a fictitious cone with a half-vertex angle of 41°, the Taylor-Maccoll theory gives the minimum Mach number for an attached shock as 2.03. The experimental results indicate that for an angle of attack of 6° the flow field behind the lower shock has a subsonic region for Mach numbers to 1.857. The lower shock for a Mach number of 1.986, however, does not have a subsonic region and thus has attached characteristics. The subsonic region for a Mach number of 1.986 does not appear until an angle of attack of 9° is reached. These subsonic regions behind the lower shock increase with increasing angle of attack. For a Mach number of 3.01, the conical shock theory predicts that shock detachment will occur at a half-vertex angle of something less than 50°, corresponding to an angle of attack of less than 15°. However, experimental results indicate that at an angle of attack of 15° the shock still has attached characteristics; no subsonic zone is present.

The upper portion of the shock can be considered in the same manner. In this case the fictitious half-vertex angle can be considered

as decreasing as the angle of attack increases. The conical shock theory predicts that at an angle of attack of approximately 6° corresponding to a half-vertex angle of 29°, the shock will become attached for the Mach numbers investigated. The experimental results indicate that, for the angles of attack investigated, if a subsonic zone initially exists it does not wholly disappear.

It therefore is apparent that interaction does exist between the upper and lower portions of the shock wave in conical flow at angles of attack. This interaction inhibits or delays the disappearance of the subsonic region behind the upper shock and delays the appearance of the subsonic region behind the lower shock as angle of attack is increased. Stated differently, this interaction decreases the ability of the shock to deflect the flow in the upper portion of the shock and increases this same ability in the lower, as compared to that predicted by the Taylor-Maccoll theory.

The cone surface pressure measurements at a Mach number of 1.584 were reduced to the non-dimensional form p_s/p_o', where p_o' is the reservoir pressure behind the normal shock. The plot of these measurements are included to indicate the variation of the cone surface pressure at angles of attack of 0° and 12°, (Cf. Fig. 27).

IV. CONCLUSIONS

The results of this investigation indicate that at angles of attack there is interaction between the upper and lower portions of the shock. This interaction tends to delay the appearance of a subsonic region behind the lower portion of the shock and to delay the disappearance of the subsonic region behind the upper portion of the shock. The delay in the disappearance is greater than the delay in the appearance.

It is also indicated that the extent of the total subsonic region is reduced as the angle of attack is increased for those Mach numbers which initially produce detached shocks.

Finally, it appears that if the shock is initially attached to the cone it remains attached even though mixed flow appears behind the shock, for the range of angles of attack tested.

REFERENCES

1. Marschner, B. W., and Altseimer, J., "An Investigation of Detached Shock Waves", Aero. Eng. Thesis, California Institute of Technology, 1948.

2. MacKinnon, N. A., and Muirhead, V. I., "Flow Field Around a Finite Cone With Shock", Aero. Eng. Thesis, California Institute of Technology, 1949.

3. Puckett, Allen E., and Schamberg, Richard, "Final Report - GALCIT Supersonic Wind Tunnel Tests", Library of Aeronautics, California Institute of Technology, June, 1946.

4. Puckett, Allen E., "Supersonic Nozzle Design", Journal of Applied Mechanics, December, 1946.

5. Dailey, C. L., and Wood, F. C., "Computation Curves for Compressible Fluid Problems", John Wiley and Sons, Inc., New York, Chapman and Hall, Limited, London.

SAMPLE CALCULATIONS

A. Determination of Mach number in test section:

p_{o_g} = gauge reservoir pressure

p_2 = reference wall static orifice pressure

p_{2_g} = gauge reference pressure

p_x = nozzle centerline static orifice pressure

Density conversion factors:

1 cm. acetylene tetrabromide = .2188 cm. hg.

1 cm. silicone = .0695 cm. hg.

$$\frac{p_x}{p_o} = \frac{p_2}{p_o} - \frac{p_2 - p_x}{p_o}$$

Orifice position	1.8"
p_{o_g}	103.0
p_a	93.3
$p_{o_g} - p_a$	9.7
$.2188\ (p_{o_g} - p_a)$	2.12
Barometer	74.57
p_o	72.45
p_a	73.15
p_{2_g}	129.6
$p_a - p_{2_g}$	56.45
p_2	18.12

p_2/p_a (av.)	.2487
p_2	69.6
p_x	64.0
$p_2 - p_x$	-5.6
$.0695\ (p_2 - p_x)$	-.389
$.0695\ (p_2 - p_x)/p_o$	-.00537
p_x/p_o	.2541
M	1.544

B. Determination of p_s/p_o', M = 1.584

p_s = surface pressure on cone

p_o' = reservoir pressure behind normal shock

$$p_s/p_o' = \frac{p_s}{p_o} \times \frac{p_o}{p_o'}$$

p_s/p_o was found in the same way as in the determination of the Mach number.

p_s/p_o	.591
p_o/p_o'	1.109
p_s/p_o'	.655
x'	.2497"
S	.32"
x'/S	.779

TABLE I

M = 1.438

$\alpha = 0^\circ$ Upper and Lower		$\alpha = 3^\circ$ Upper		$\alpha = 3^\circ$ Lower	
Y/D	M_2	Y/D	M_2	Y/D	M_2
0	.730	0	.730	0	.736
.2	.780	.2	.808	.03	.735
.4	.825	.4	.865	.2	.769
.6	.865	.6	.895	.4	.822
.8	.905	.8	.942	.6	.865
1.0	.942	1.0	.990	.8	.900
1.2	.974	1.12	1.000	1.0	.927
1.4	.999			1.2	.958
1.41	1.000			1.4	.991
				1.47	1.000

TABLE I (continued)

M = 1.438

$\alpha = 6^{\circ}$				$\alpha = 9^{\circ}$			
Upper		Lower		Upper		Lower	
Y/D	M_2	Y/D	M_2	Y/D	M_2	Y/D	M_2
0	.748	0	.748	0	.750	0	.750
.2	.800	.04	.735	.2	.835	.09	.735
.4	.885	.2	.760	.4	.895	.2	.765
.6	.920	.4	.817	.6	.920	.4	.795
.8	.960	.6	.860	.8	.955	.6	.815
1.0	.990	.8	.900	1.0	.990	.8	.838
1.08	1.000	1.0	.934	1.02	1.000	1.0	.862
		1.2	.960			1.2	.900
		1.4	.985			1.4	.942
		1.58	1.000			1.59	1.000

TABLE I (continued)

M = 1.438

$\alpha = 12^{\circ}$				$\alpha = 15^{\circ}$			
Upper		Lower		Upper		Lower	
Y/D	M_2	Y/D	M_2	Y/D	M_2	Y/D	M_2
0	.770	0	.770	0	.812	0	.812
.2	.850	.12	.735	.2	.880	.185	.735
.4	.920	.2	.750	.4	.940	.2	.735
.6	.930	.4	.775	.6	.985	.4	.760
.8	.990	.6	.797	.735	1.000	.6	.798
.85	1.000	.8	.860			.8	.845
		1.0	.890			1.0	.894
		1.2	.943			1.2	.937
		1.4	.995			1.4	.975
		1.44	1.000			1.57	1.000

TABLE II

M = 1.544

$\alpha = 0^\circ$		$\alpha = 3^\circ$			
Upper and Lower		Upper		Lower	
Y/D	M_2	Y/D	M_2	Y/D	M_2
0	.695	0	.700	0	.700
.2	.855	.2	.828	.02	.695
.4	.887	.4	.860	.2	.770
.6	.895	.6	.920	.4	.832
.8	.922	.8	.955	.6	.880
1.0	.970	.98	1.000	.8	.920
1.15	1.000			1.0	.958
				1.17	1.000

TABLE II (continued)

M = 1.544

$\alpha = 6^\circ$				$\alpha = 9^\circ$			
Upper		Lower		Upper		Lower	
Y/D	M_2	Y/D	M_2	Y/D	M_2	Y/D	M_2
0	.707	0	.707	0	.720	0	.720
.2	.804	.02	.695	.2	.770	.08	.695
.4	.905	.2	.775	.4	.775	.2	.745
.6	.938	.4	.843	.6	.946	.4	.820
.8	.963	.6	.885	.8	.992	.6	.856
1.0	.993	.8	.910	.88	1.000	.8	.900
1.02	1.000	1.0	.960			1.0	.951
		1.12	1.000			1.18	1.000

TABLE II (continued)

M = 1.544

$\alpha = 12^\circ$				$\alpha = 15^\circ$			
Upper		Lower		Upper		Lower	
Y/D	M_2	Y/D	M_2	Y/D	M_2	Y/D	M_2
0	.730	0	.730	0	.740	0	.740
.2	.910	.075	.695	.2	.825	.1	.695
.4	.953	.2	.730	.4	.965	.2	.710
.68	1.000	.4	.780	.47	1.000	.4	.770
		.6	.835			.6	.827
		.8	.876			.8	.882
		1.0	.925			1.0	.934
		1.2	1.000			1.2	.990
						1.22	1.000

TABLE III

M = 1.584

$\alpha = 0^\circ$		$\alpha = 3^\circ$			
Upper and Lower		Upper		Lower	
Y/D	M_2	Y/D	M_2	Y/D	M_2
0	.685	0	.690	0	.690
.2	.867	.2	.912	.02	.685
.4	.912	.4	.952	.2	.815
.6	.925	.6	.960	.4	.880
.8	.949	.8	.990	.6	.918
.94	1.000	.83	1.000	.8	.953
				1.0	.980
				1.06	1.000

TABLE III (continued)

M = 1.584

$\alpha = 6^\circ$				$\alpha = 9^\circ$			
Upper		Lower		Upper		Lower	
Y/D	M_2	Y/D	M_2	Y/D	M_2	Y/D	M_2
0	.695	0	.695	0	.705	0	.705
.2	.940	.02	.685	.2	.990	.08	.685
.4	.947	.2	.800	.4	.996	.2	.735
.6	.969	.4	.830	.55	1.000	.4	.800
.75	1.000	.6	.853			.6	.846
		.8	.933			.8	.900
		1.0	.990			1.0	.968
		1.035	1.000			1.17	1.000

TABLE III (continued)

M = 1.584

$\alpha = 12^\circ$				$\alpha = 15^\circ$			
Upper		Lower		Upper		Lower	
Y/D	M_2	Y/D	M_2	Y/D	M_2	Y/D	M_2
0	.700	0	.715	0	.730	0	.730
.2	.970	.07	.685	.2	.975	.08	.685
.3	1.000	.2	.732	.23	1.000	.2	.740
		.4	.790			.4	.780
		.6	.837			.6	.800
		.8	.885			.8	.851
		1.0	.958			1.0	.920
		1.16	1.000			1.14	1.000

TABLE IV

M = 1.857

$\alpha = 0^\circ$

Upper and Lower

Supersonic

$\alpha = 3^\circ$

Upper and Lower

Supersonic

$\alpha = 6^\circ$

Upper	Lower	
	Y/D	M_2
Supersonic	0	.755
	.2	.890
	.4	.970
	.6	.995
	.62	1.000

$\alpha = 9^\circ$

Upper	Lower	
	Y/D	M_2
Supersonic	0	.830
	.2	.850
	.4	.920
	.6	.970
	.67	1.000

TABLE IV (continued)

M = 1.857

$\alpha = 12^{\circ}$			$\alpha = 15^{\circ}$		
Upper	Lower		Upper	Lower	
	Y/D	M_2		Y/D	M_2
Supersonic	0	.70	Supersonic	0	.625
	.2	.78		.2	.760
	.4	.85		.4	.790
	.6	.93		.6	.867
	.75	1.00		.8	.970
				.83	1.000

TABLE V

M = 1.986

$\alpha = 0^{\circ}$

Upper and Lower

Supersonic

$\alpha = 3^{\circ}$

Upper and Lower

Supersonic

$\alpha = 6^{\circ}$

Upper and Lower

Supersonic

$\alpha = 9^{\circ}$

Upper	Lower	
	Y/D	M_2
Supersonic	0	.960
	.2	.960
	.4	.960
	.6	.972
	.64	1.000

$\alpha = 12^{\circ}$

Upper	Lower	
	Y/D	M_2
Supersonic	0	.830
	.2	.860
	.4	.895
	.6	.970
	.68	1.000

$\alpha = 15^{\circ}$

Upper	Lower	
	Y/D	M_2
Supersonic	0	.790
	.2	.810
	.4	.845
	.6	.866
	.775	1.000

TABLE VI

M = 3.01

Flow was supersonic behind shock

at all angle of attack investigated.

TABLE VII

CONDITION OF SHOCK

		0°	3°	6°	9°	12°	15°
M = 1.438	Upper	D	D	D	D	D	D
	Lower	D	D	D	D	D	D
M = 1.544	Upper	D	D	D	D	D	D
	Lower	D	D	D	D	D	D
M = 1.584	Upper	D	D	D	D	D	D
	Lower	D	D	D	D	D	D
M = 1.857	Upper	A	A	A	A	A	A
	Lower	A	A	D	D	D	D
M = 1.986	Upper	A	A	A	A	A	A
	Lower	A	A	A	D	D	D
M = 3.01	Upper	A	A	A	A	A	A
	Lower	A	A	A	A	A	A

Note: D detached shock characteristics

A attached shock characteristics

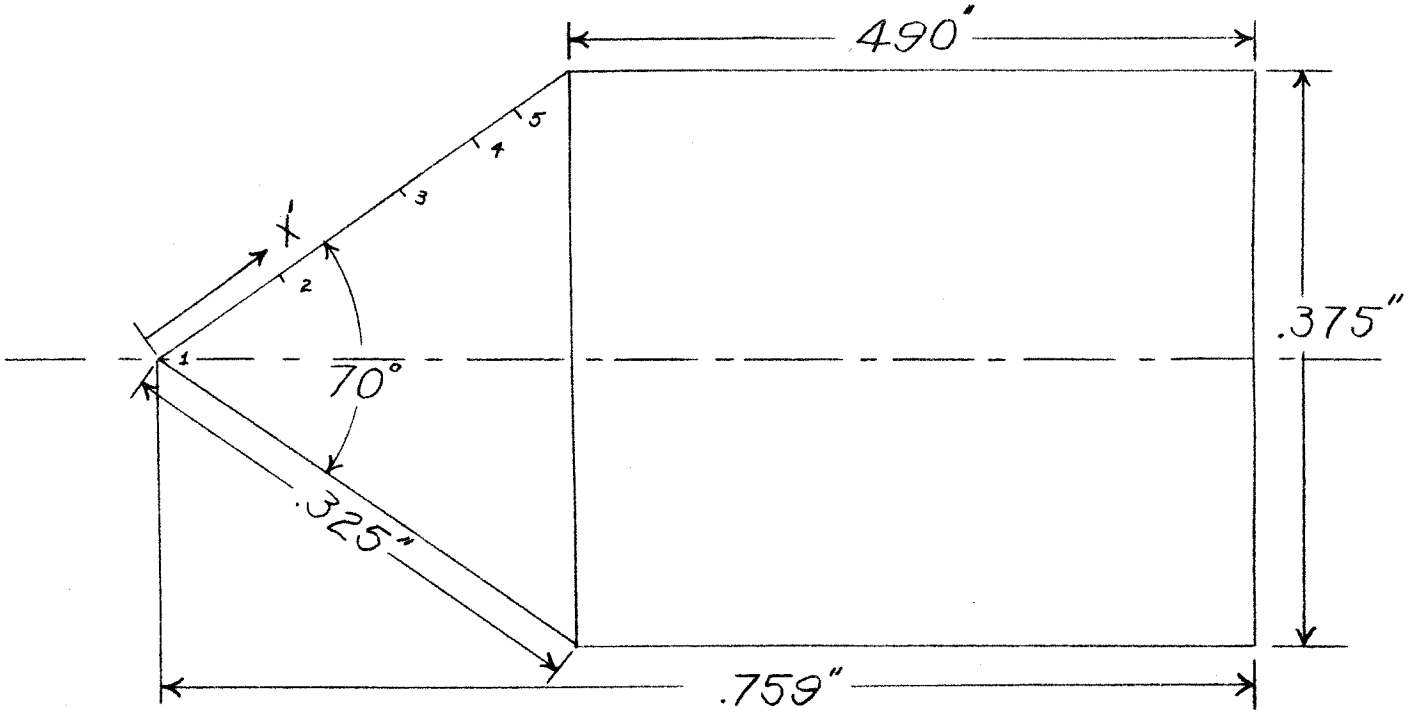

FIG. 1

PRESSURE ORIFICE LOCATION ON MODELS

Scale 8" = 1"

Cone No.	X'
1	.000"
2	.097"
3	.193"
4	.250"
5	.284"

FIG. 2
SYMBOLS

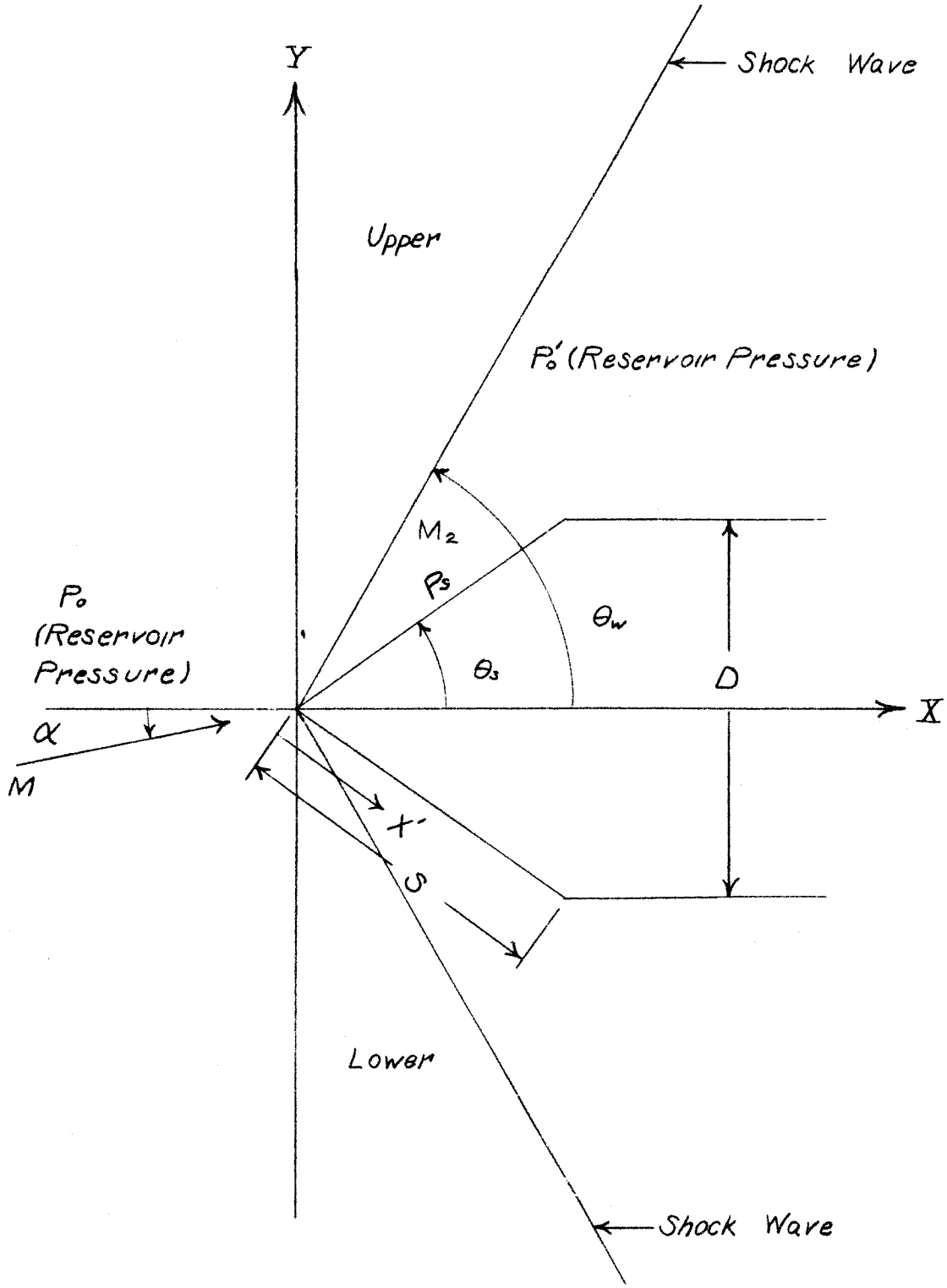

FIG. 3
M = 1.438
LOWER

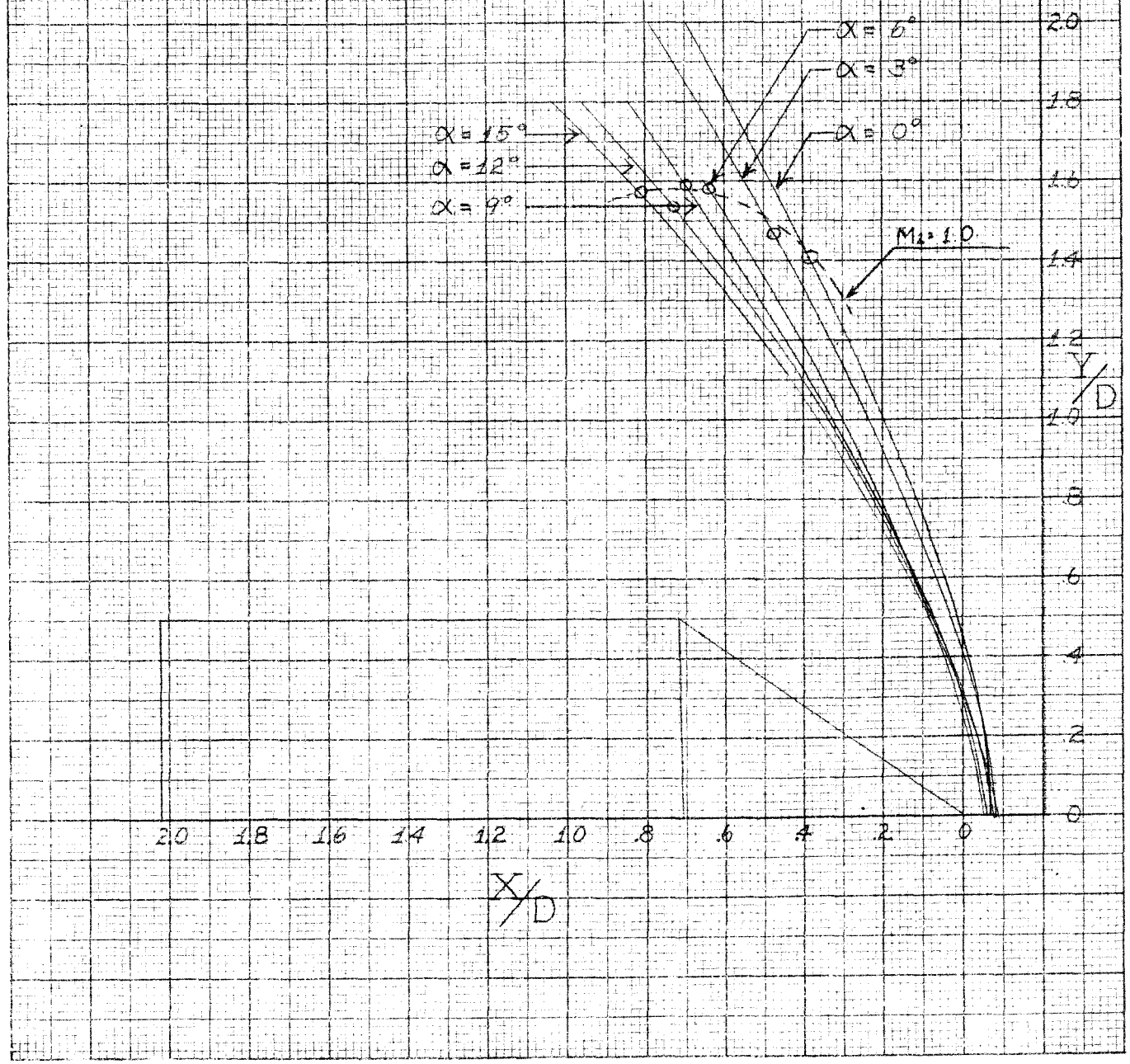

FIG. 4
M = 1.438
UPPER

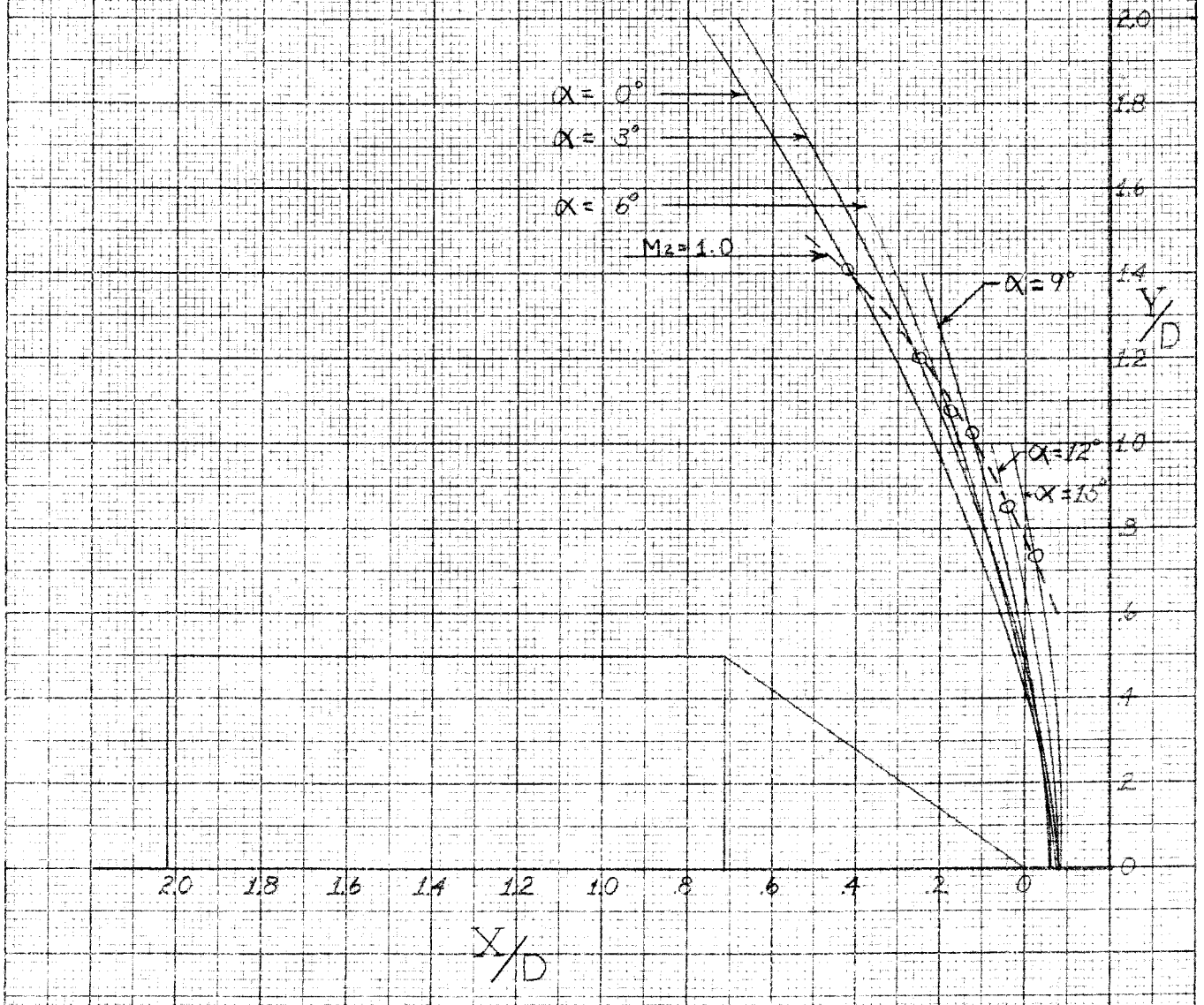

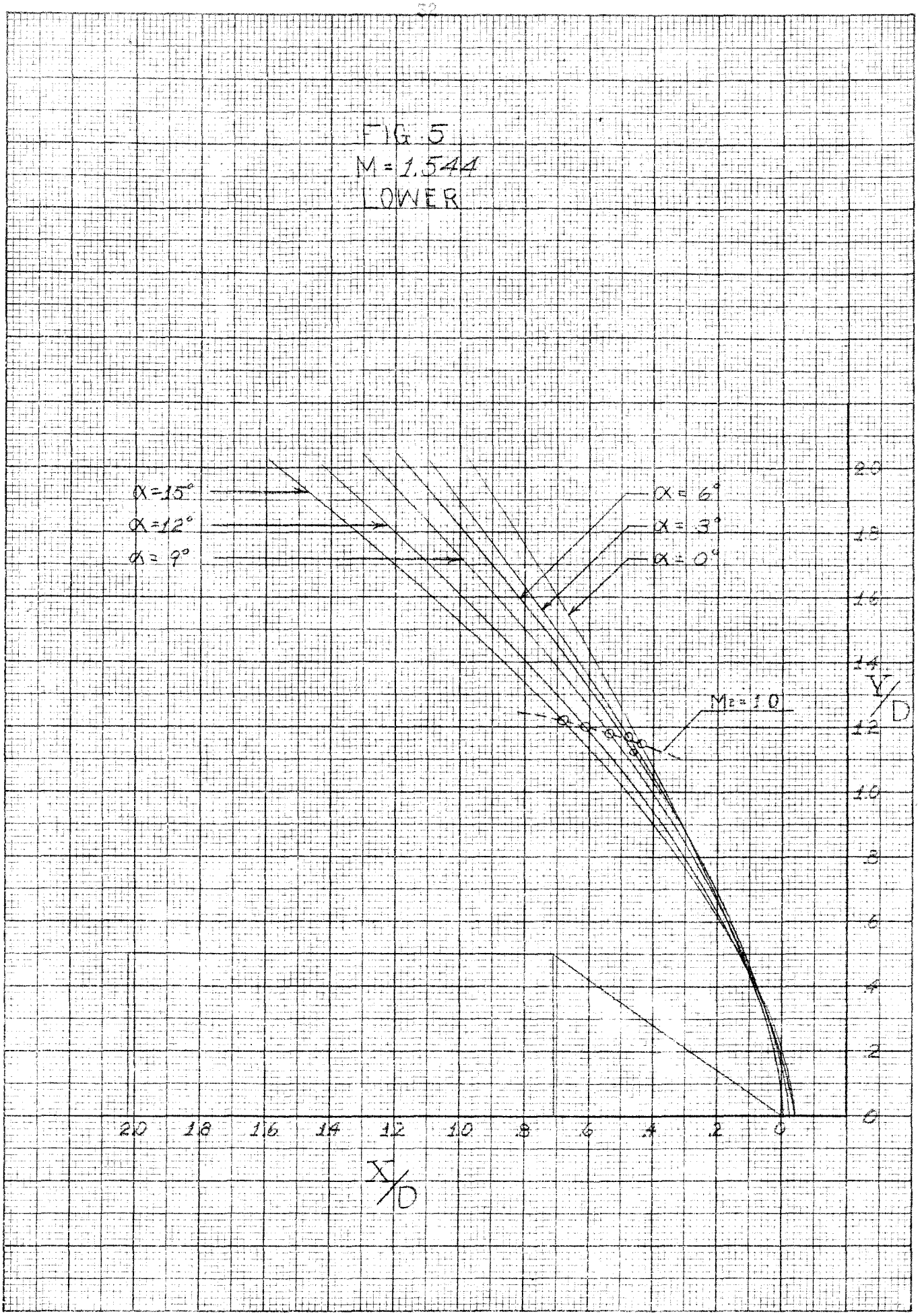
FIG. 5
M = 1.544
LOWER
α = 15°
α = 12°
α = 9°
α = 6°
α = 3°
α = 0°
M₂ = 1.0
Y/D
X/D
2.0
1.8
1.6
1.4
1.2
1.0
.8
.6
.4
.2
0

FIG. 6
M = 1.544
UPPER

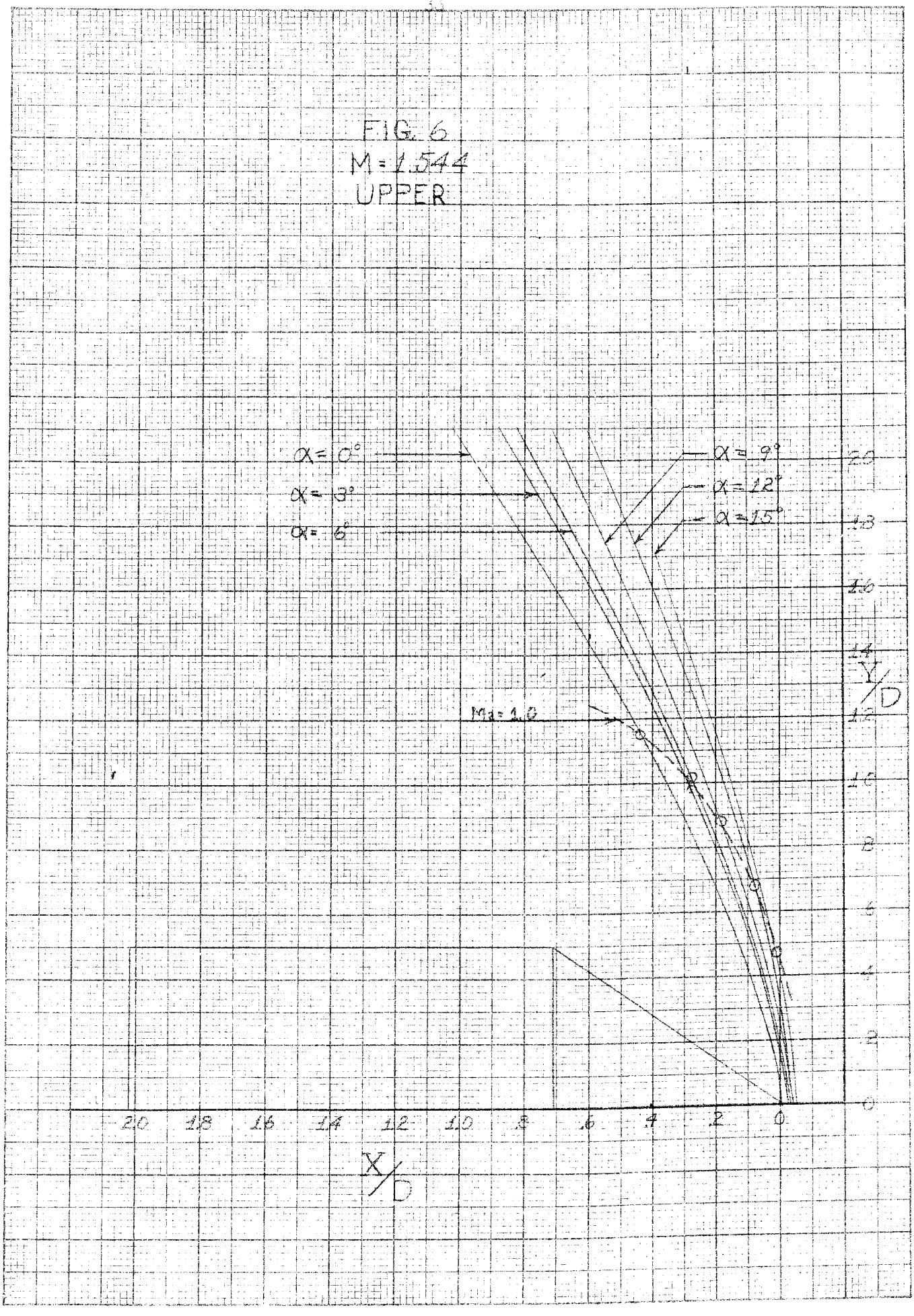

FIG. 7
M = 1.584
LOWER

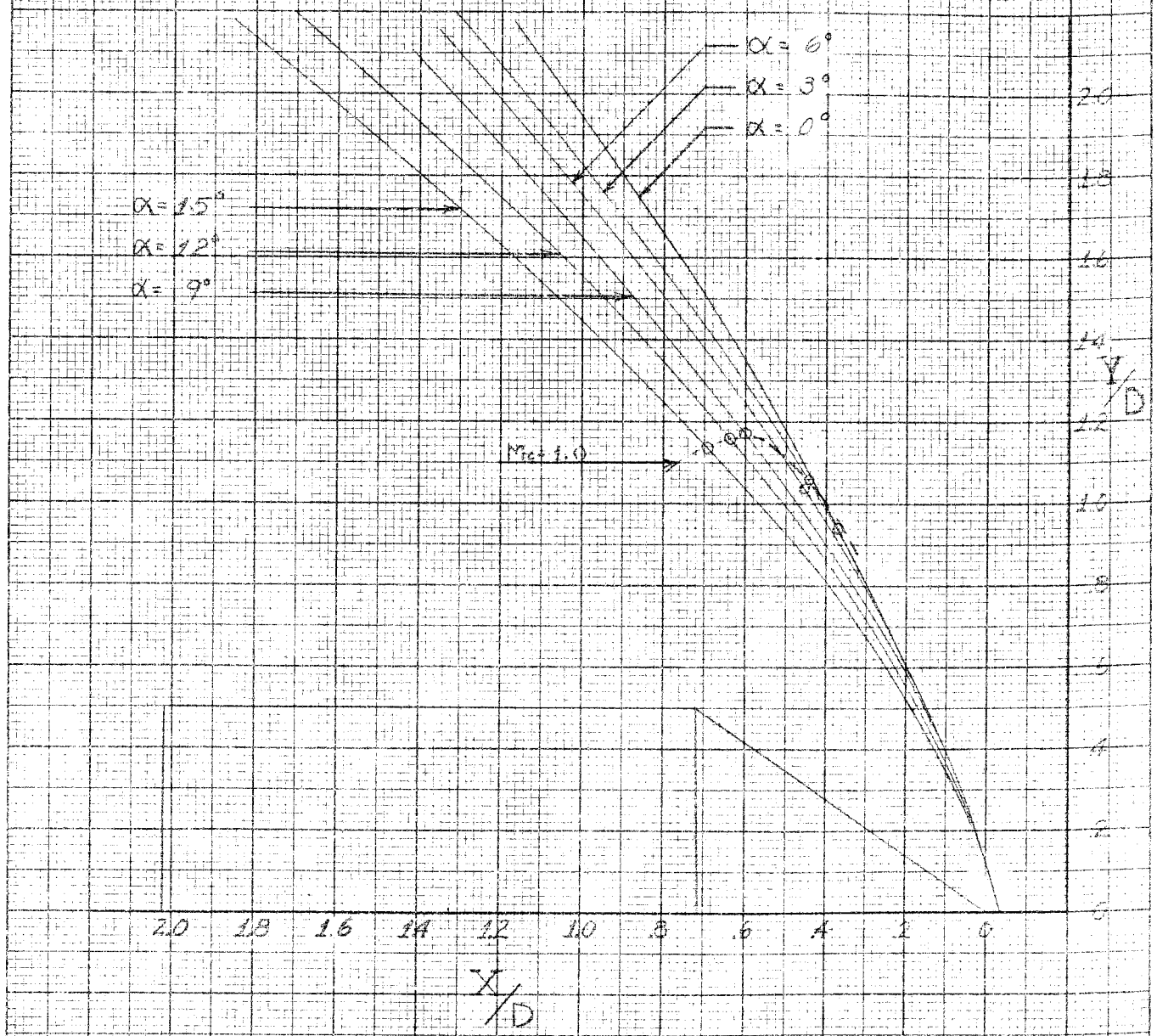

FIG. 8
M = 1.584
UPPER

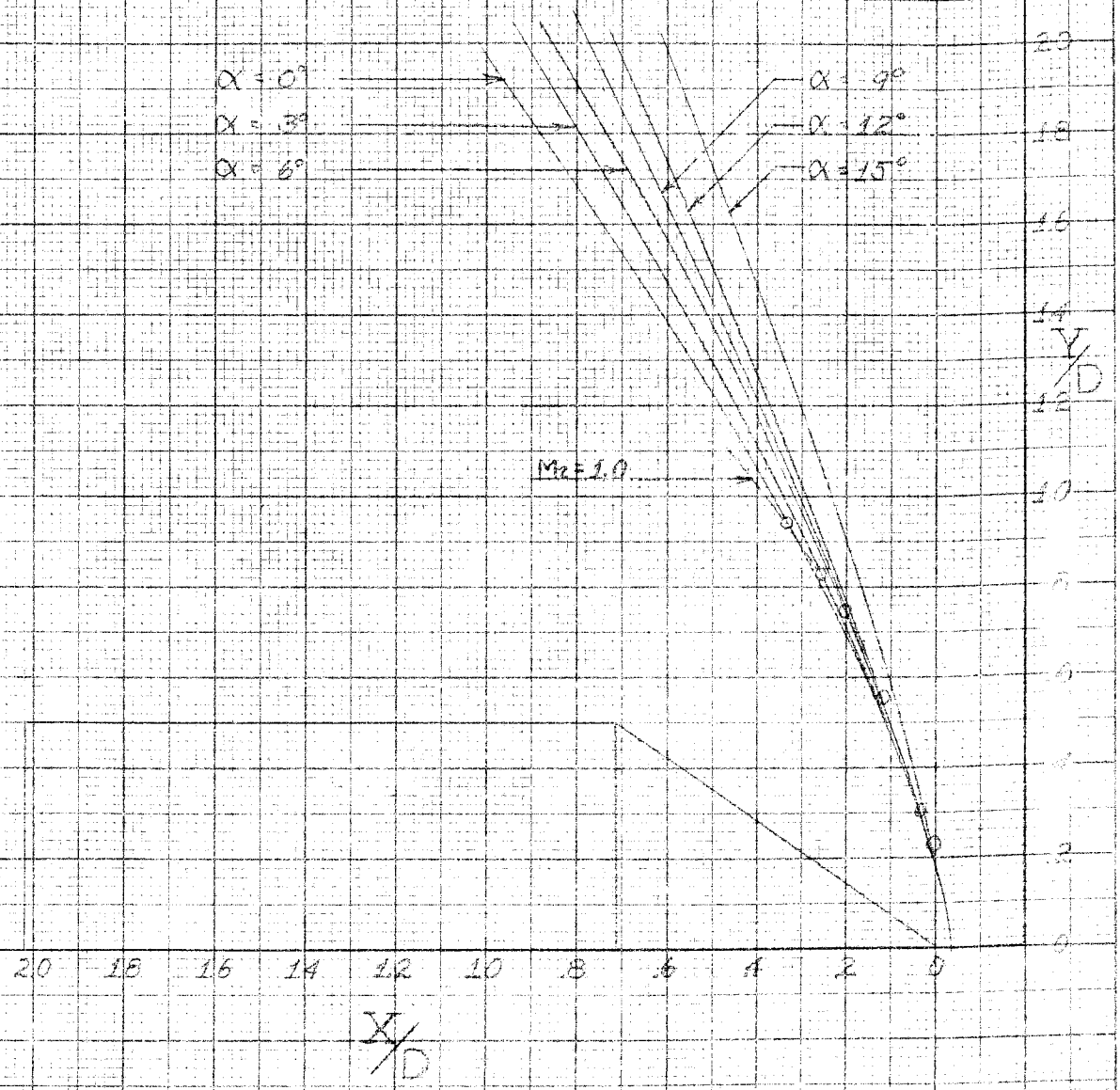

FIG. 9
M = 1.857
LOWER

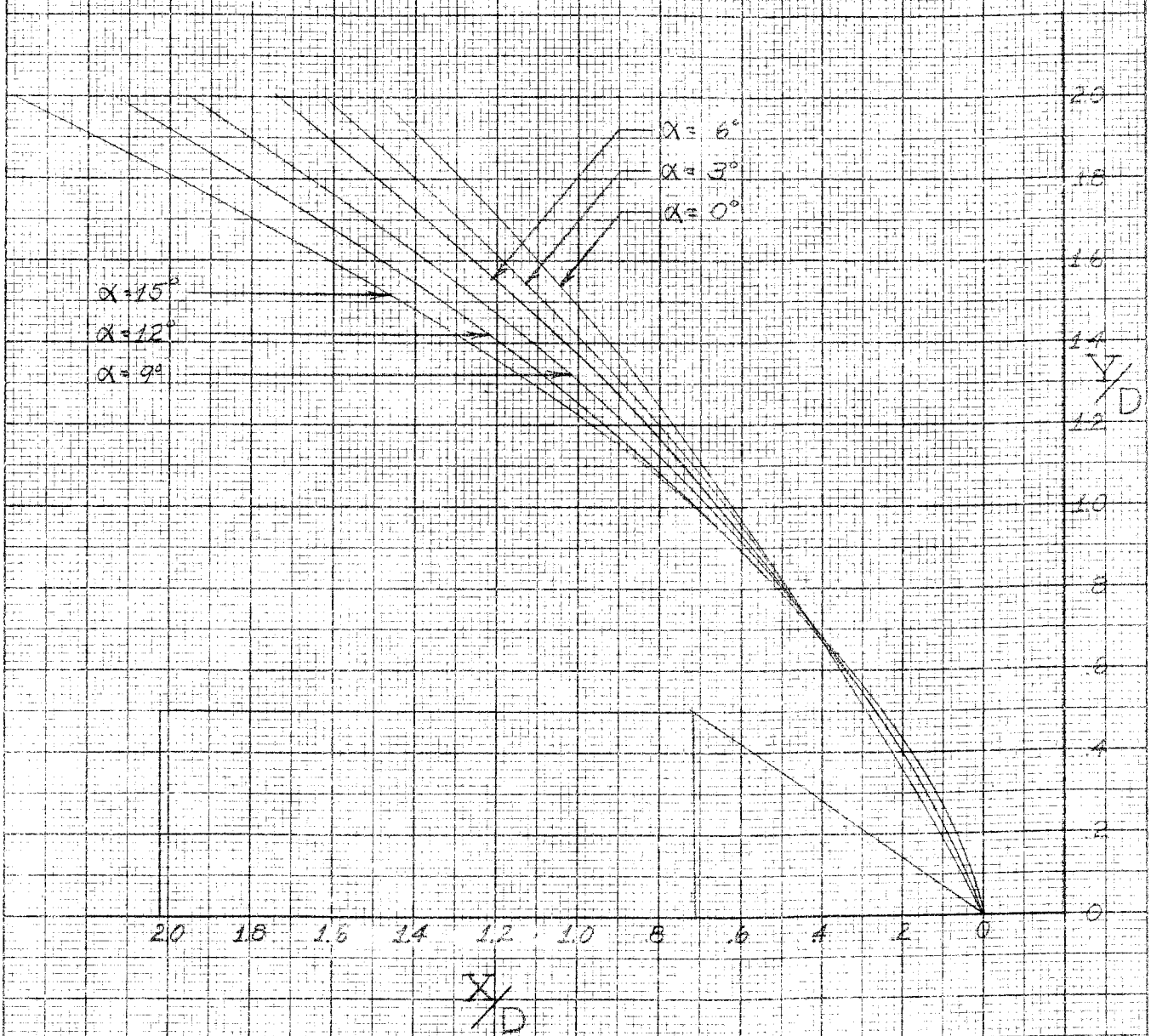

FIG 10
M = 1.857
UPPER

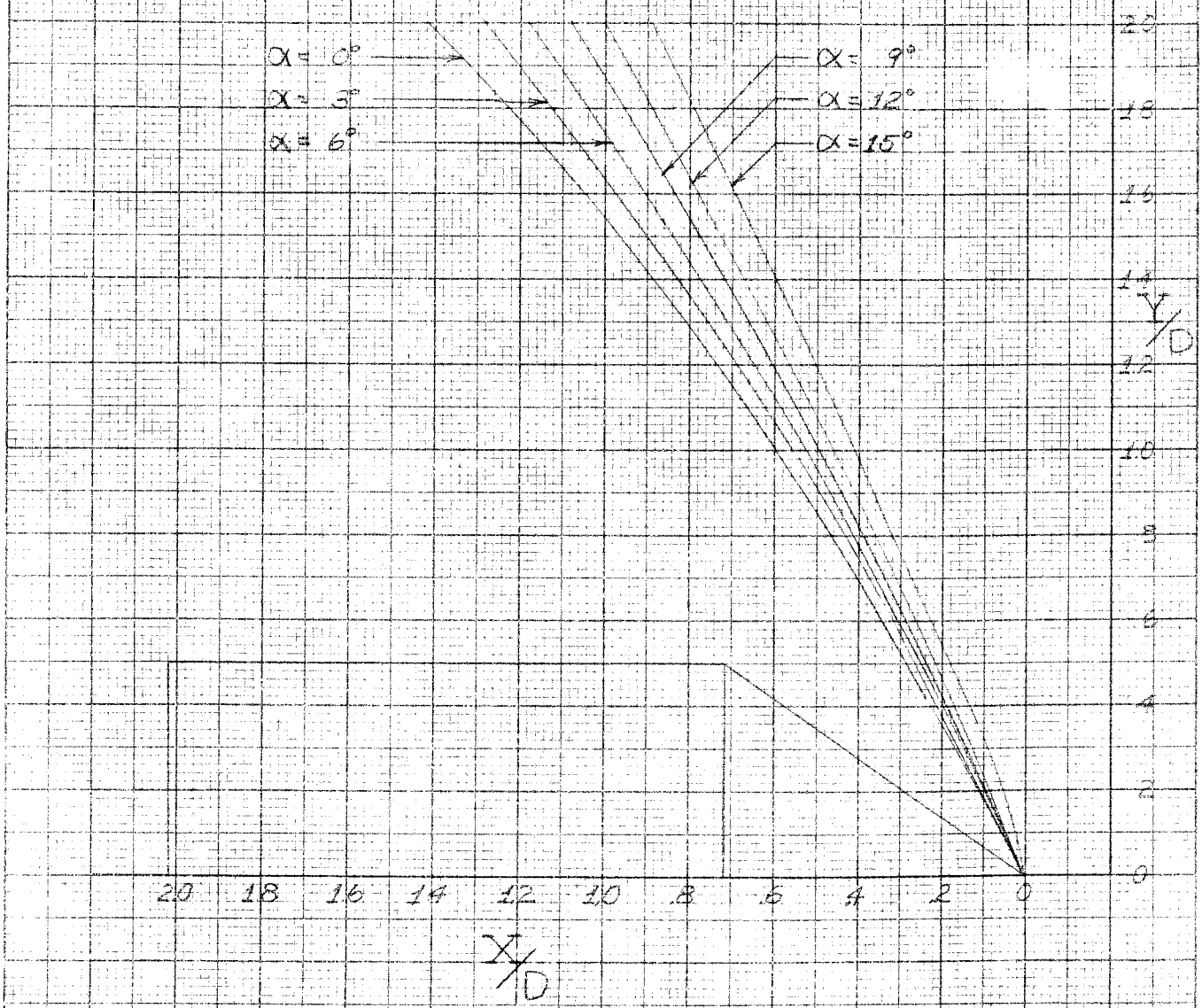

FIG. 11
M = 1.986
LOWER

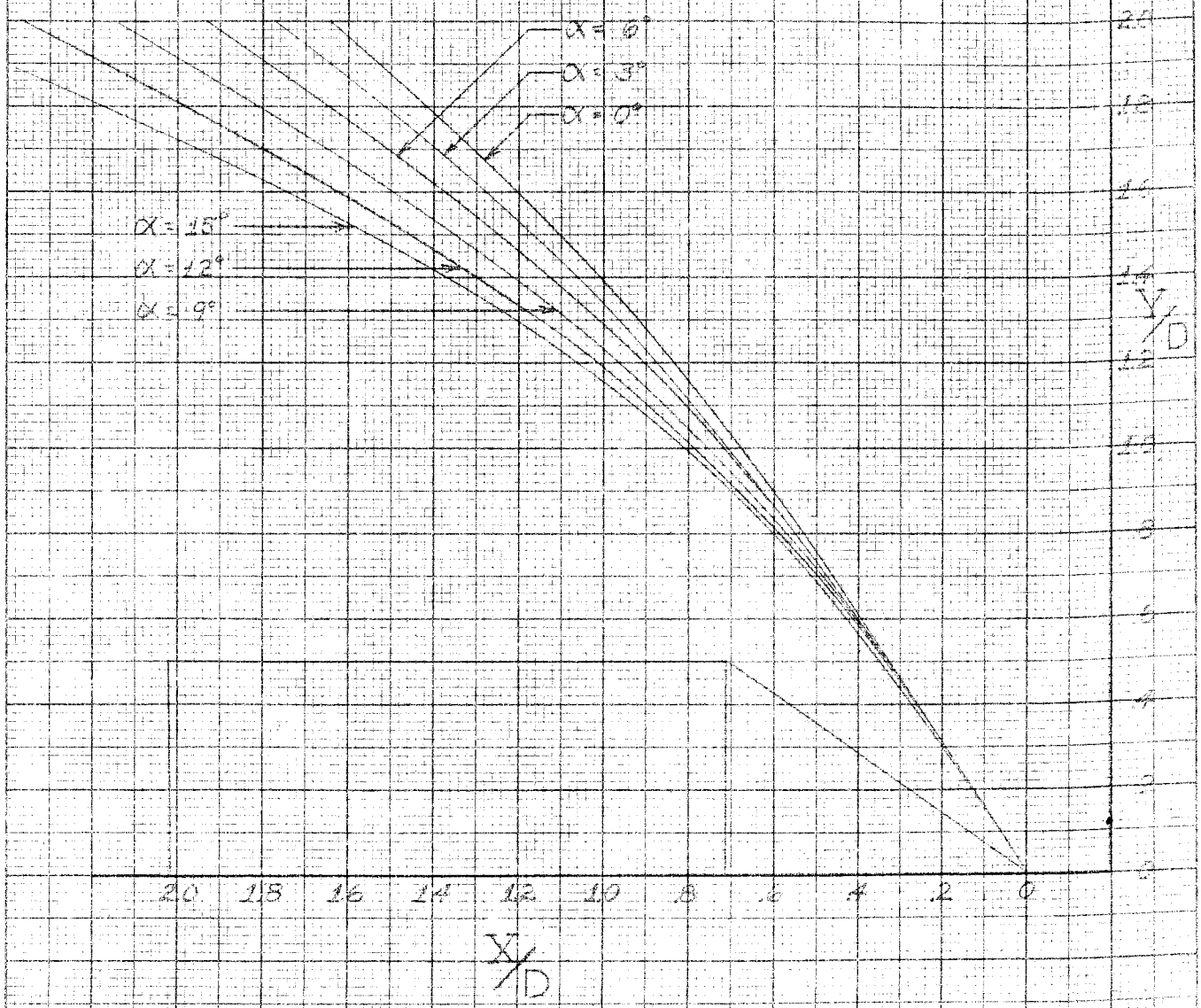

FIG 12
M = 1.986
UPPER

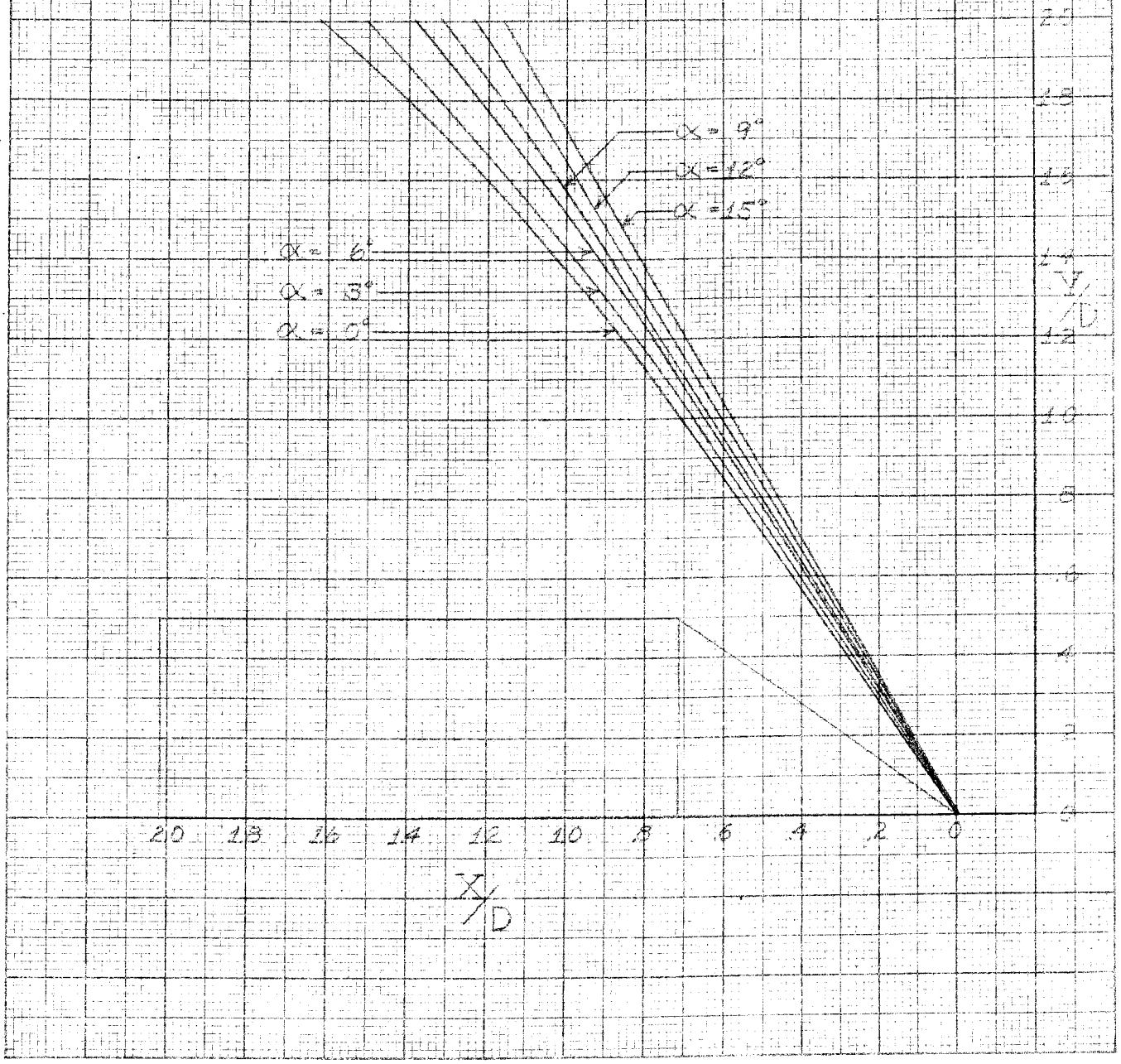

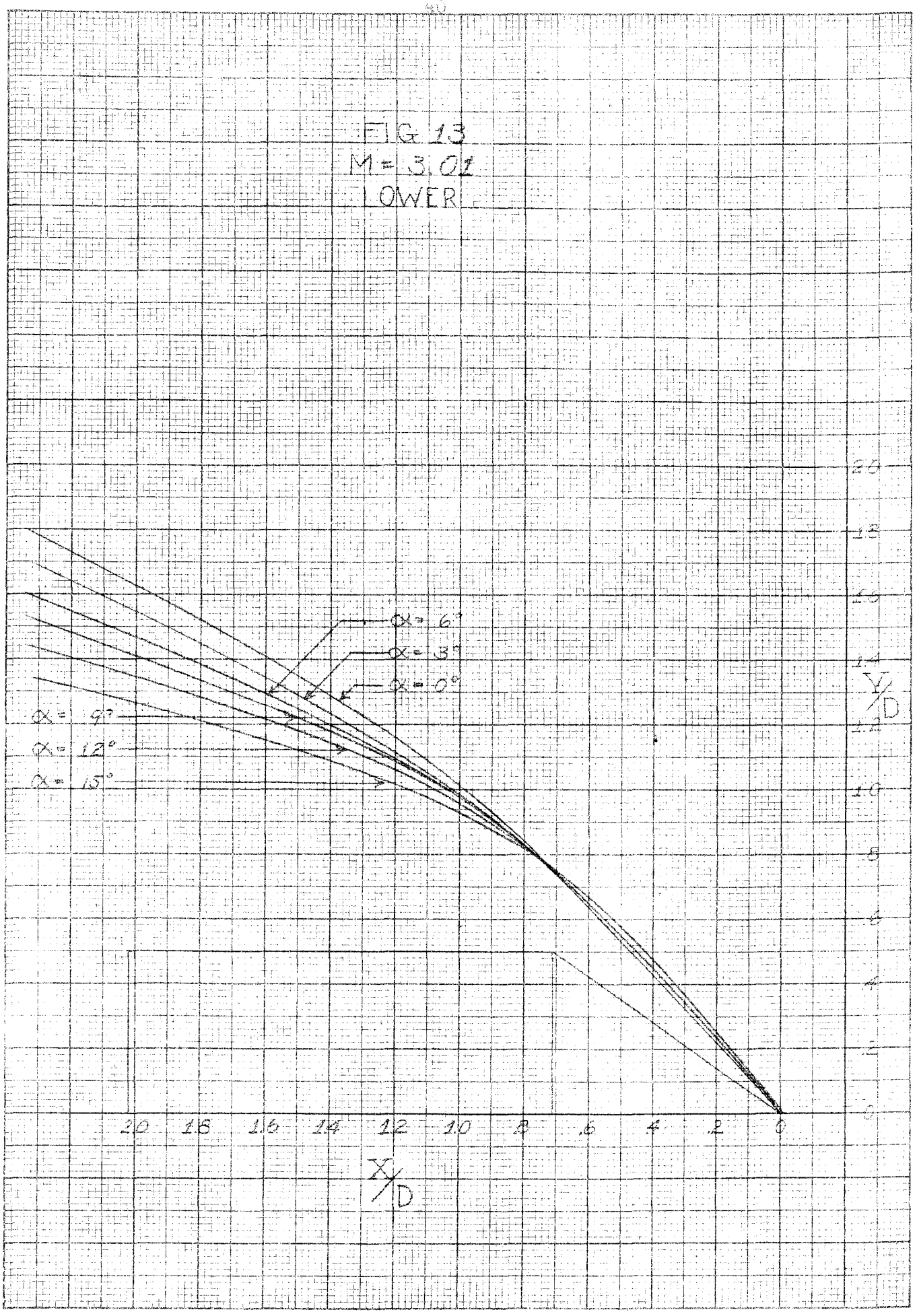
FIG 13
M = 3.01
LOWER
α = 6°
α = 3°
α = 0°
α = 9°
α = 12°
α = 15°
Y/D
X/D
2.0
1.8
1.6
1.4
1.2
1.0
.8
.6
.4
.2
0
2.0
1.8
1.6
1.4
1.2
1.0
.8
.6
.4
.2
0

FIG 14
M = 3.01
UPPER

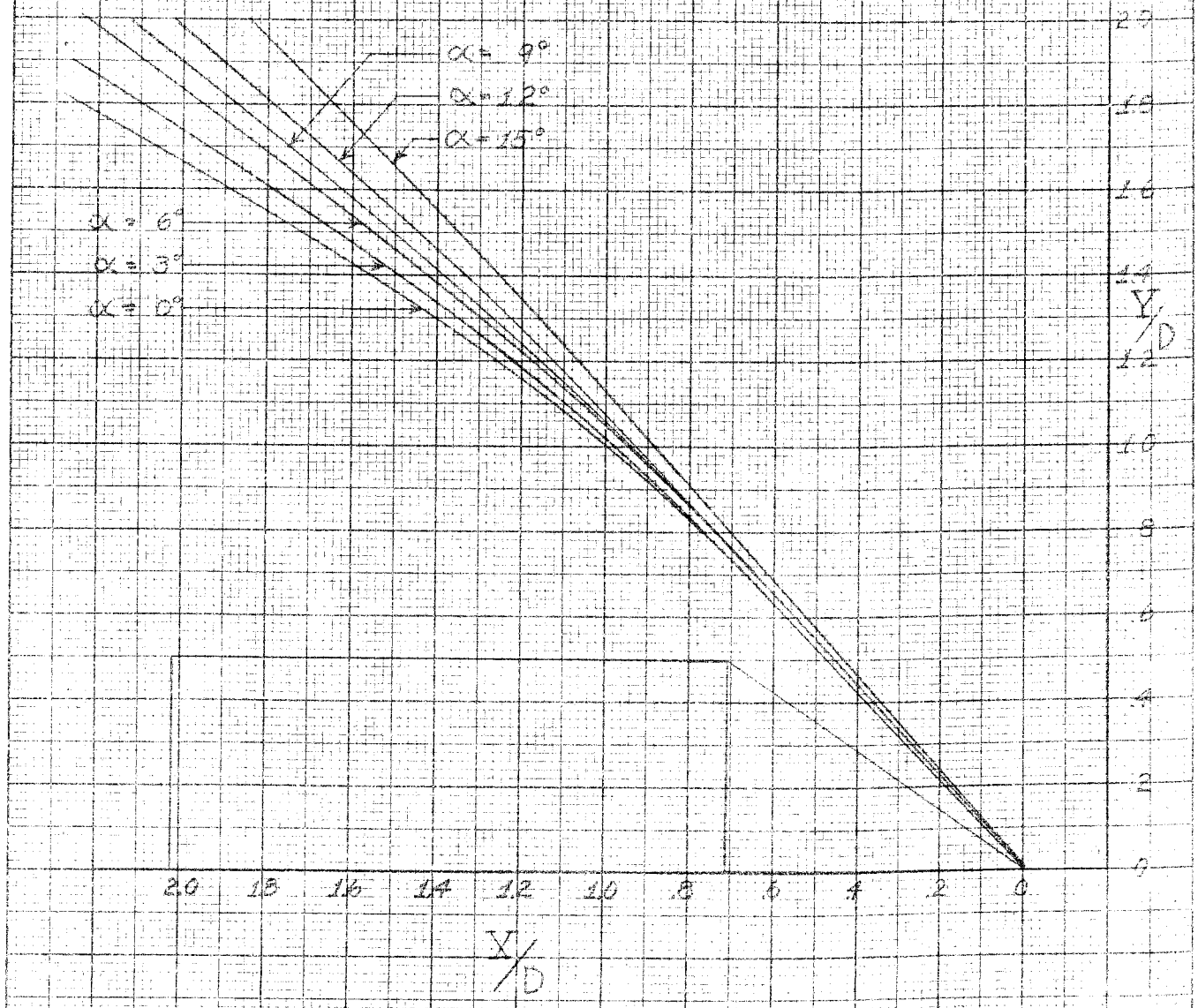

Fig. 15
$\alpha = 0°$
UPPER AND LOWER

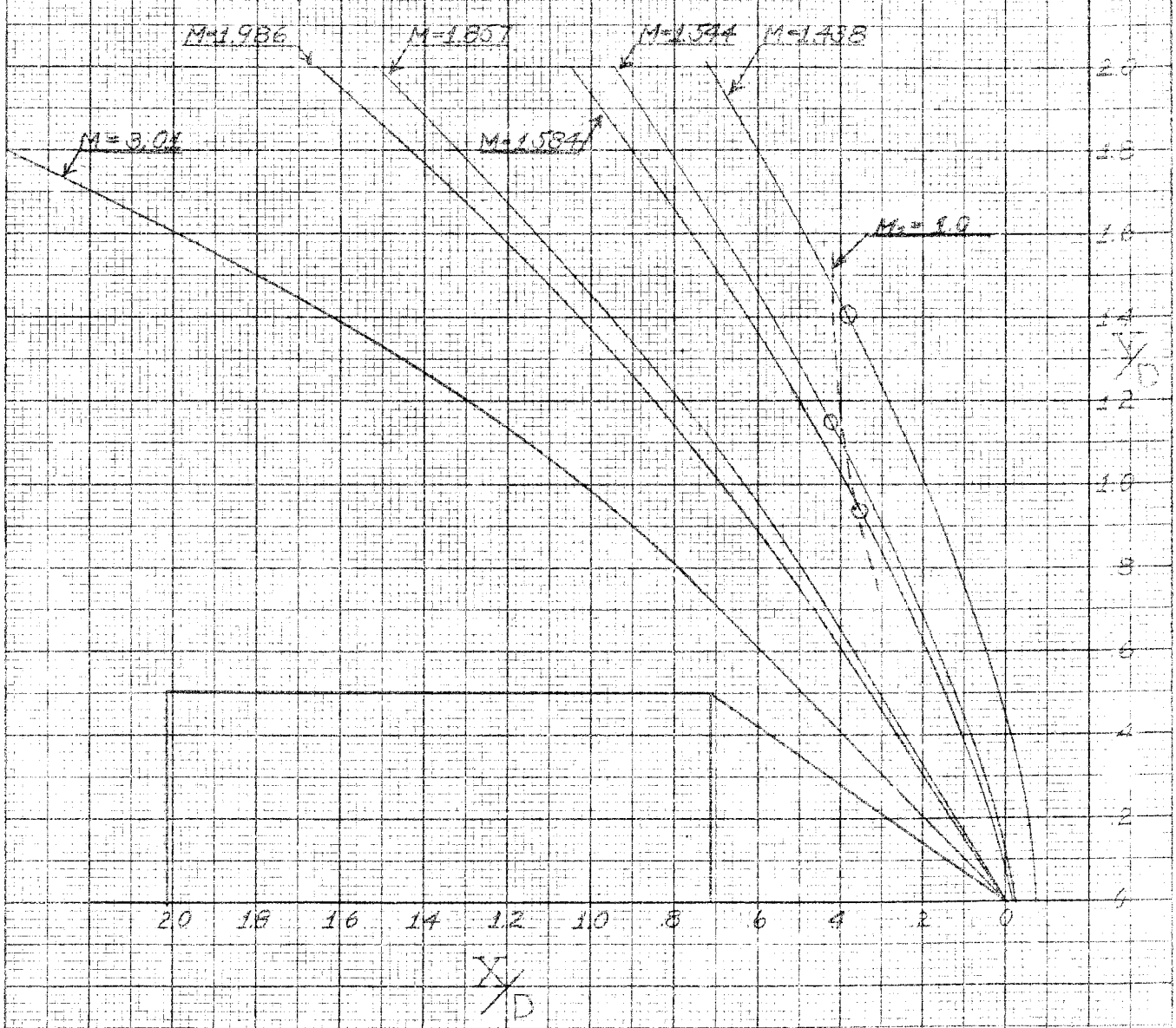

FIG 16
$\alpha = 3°$
LOWER

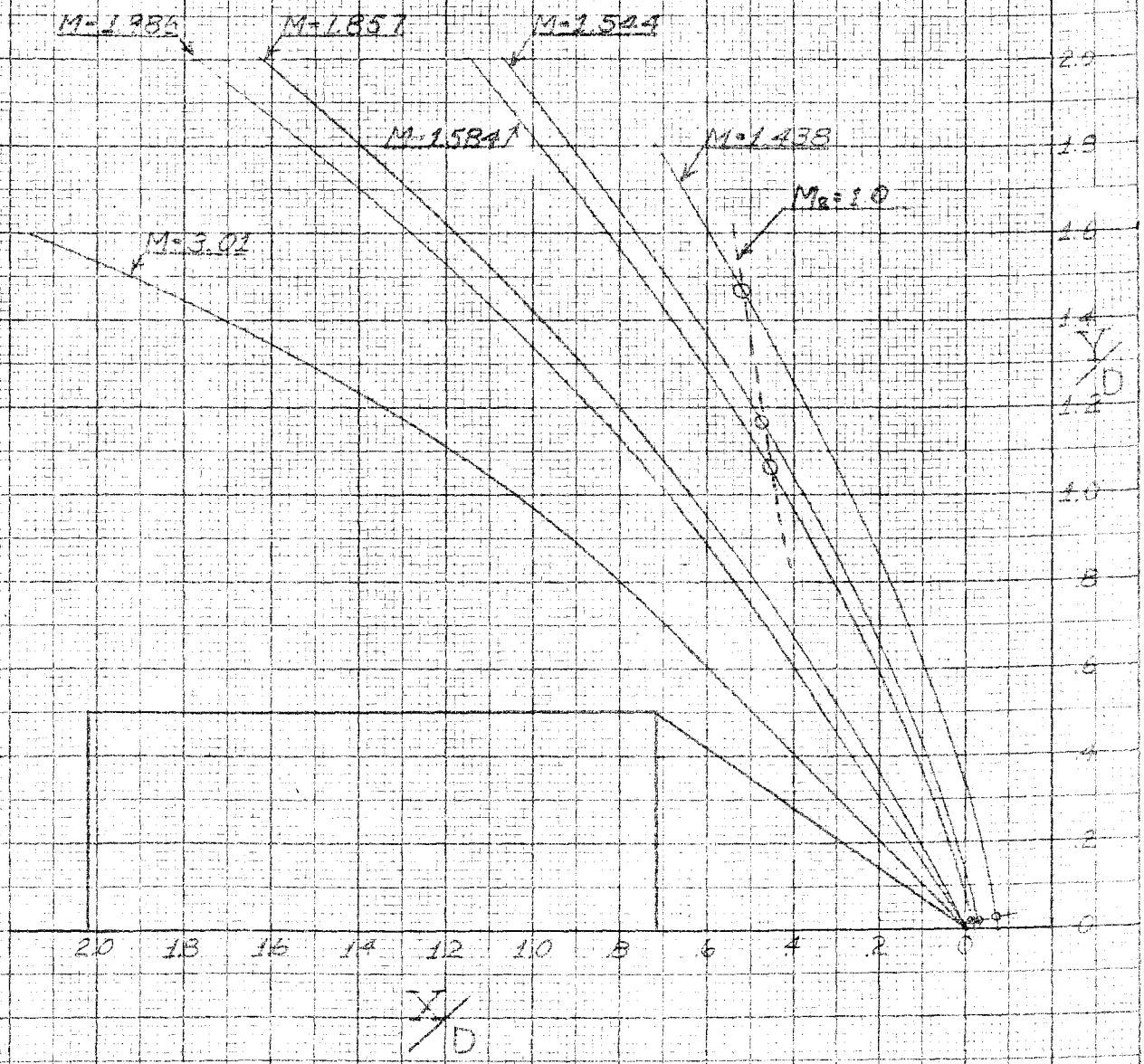

FIG. 17
$\alpha = 3°$
UPPER

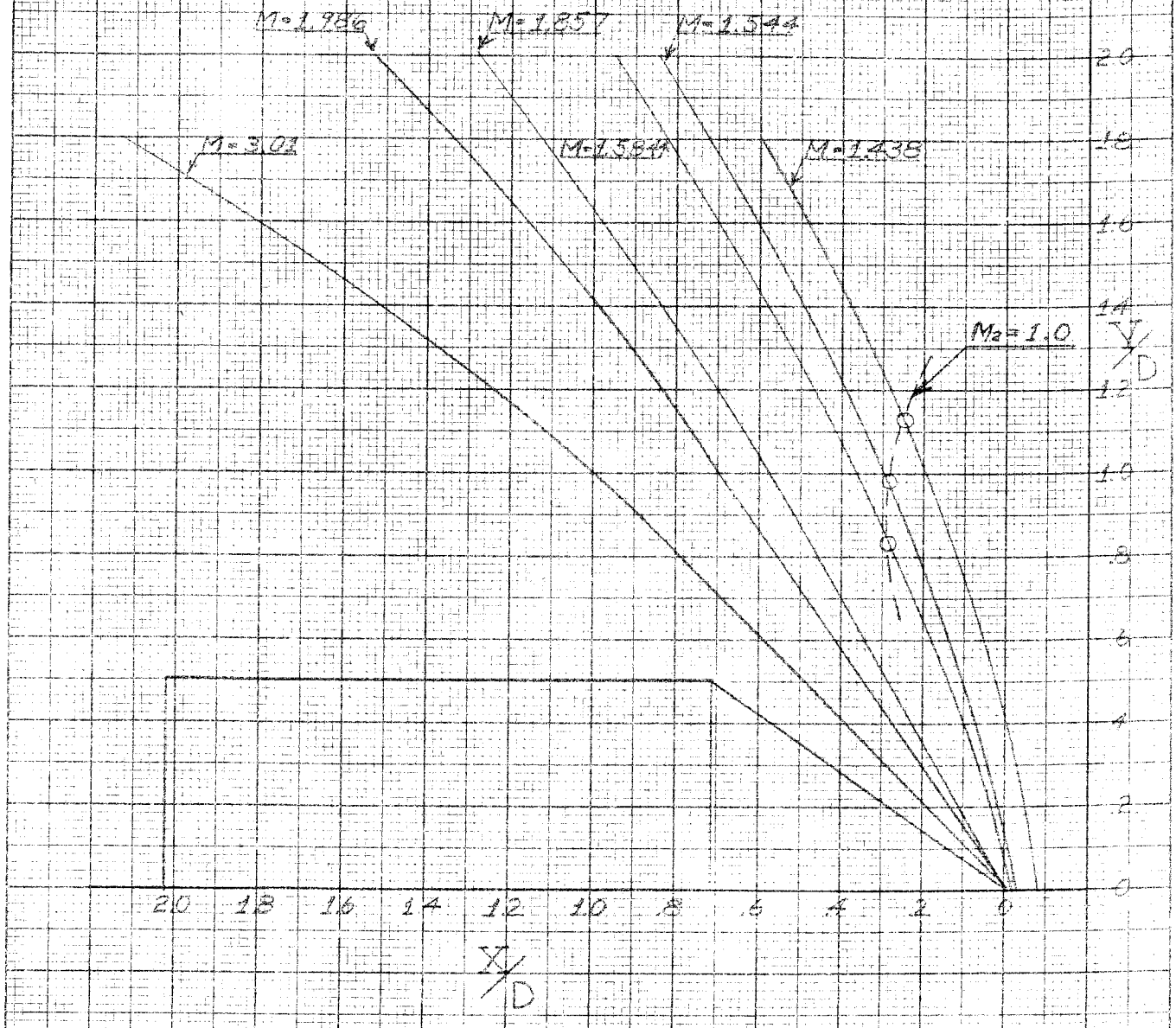

FIG. 18
$\alpha = 6°$
LOWER

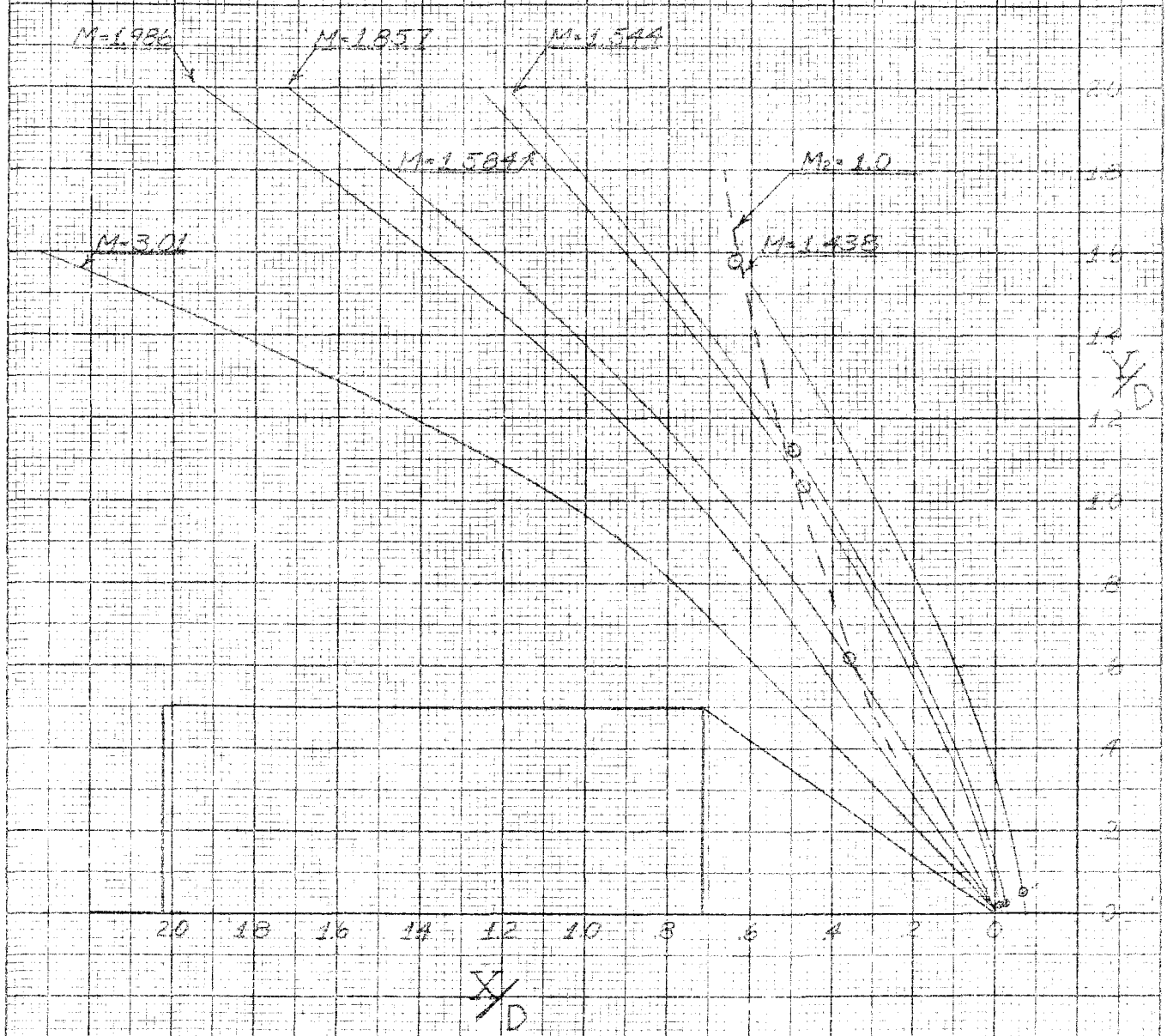

FIG. 19
$\alpha = 6°$
UPPER

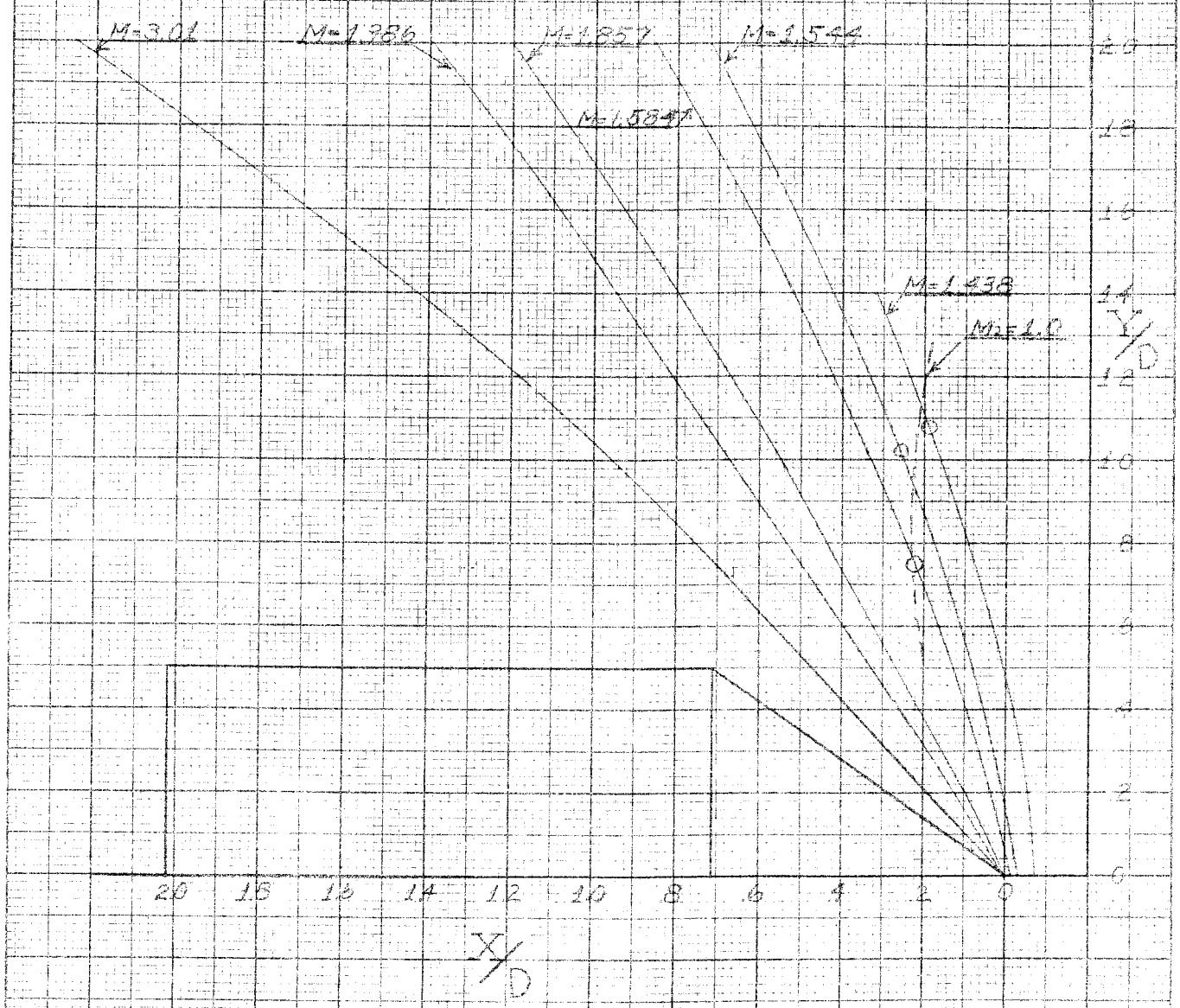

FIG 20
$\alpha = 9°$
LOWER

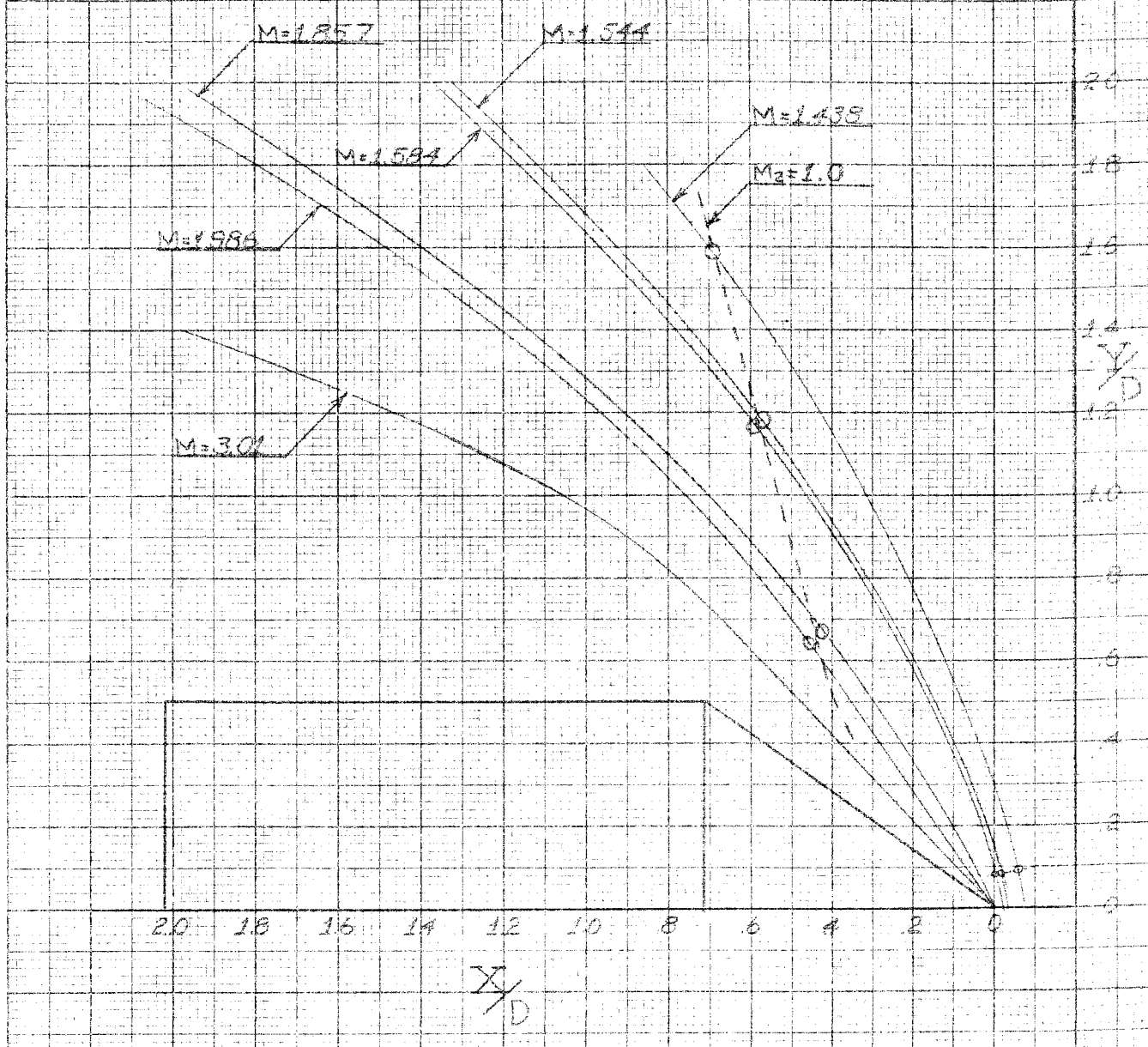

FIG 21
$\alpha = 9°$
UPPER

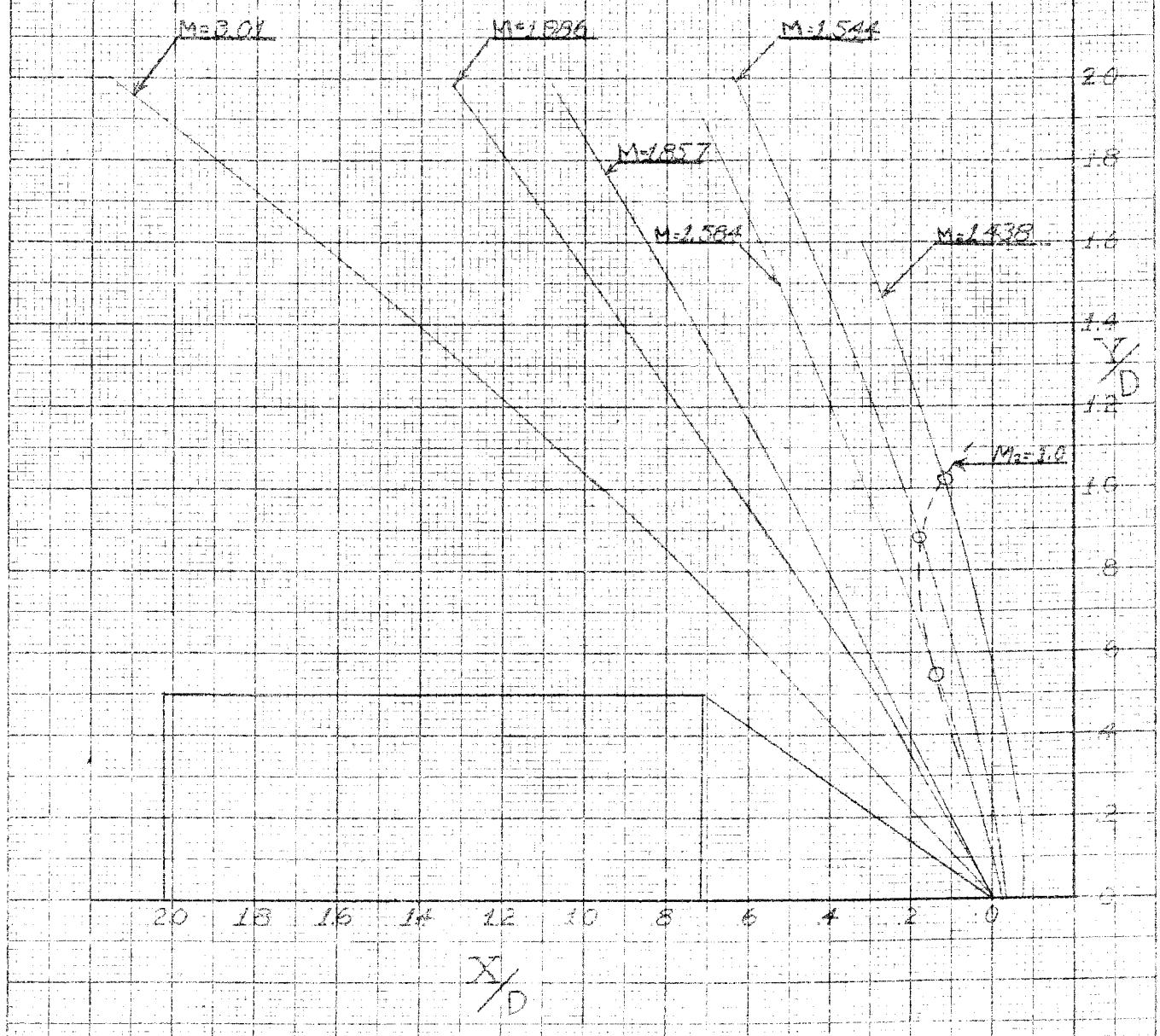

FIG 22
$\alpha = 12°$
LOWER

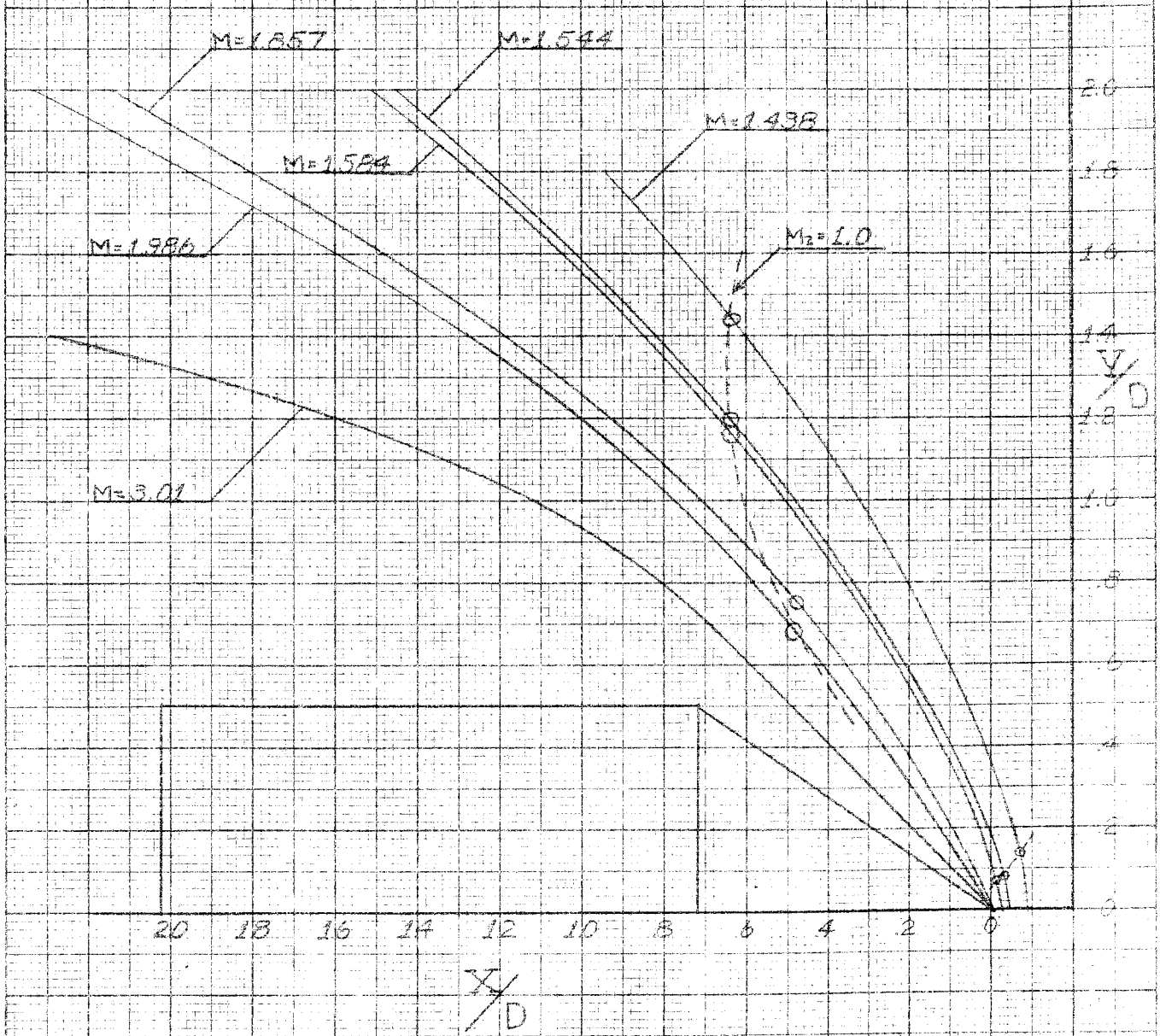

FIG 23
$\alpha = 12°$
UPPER

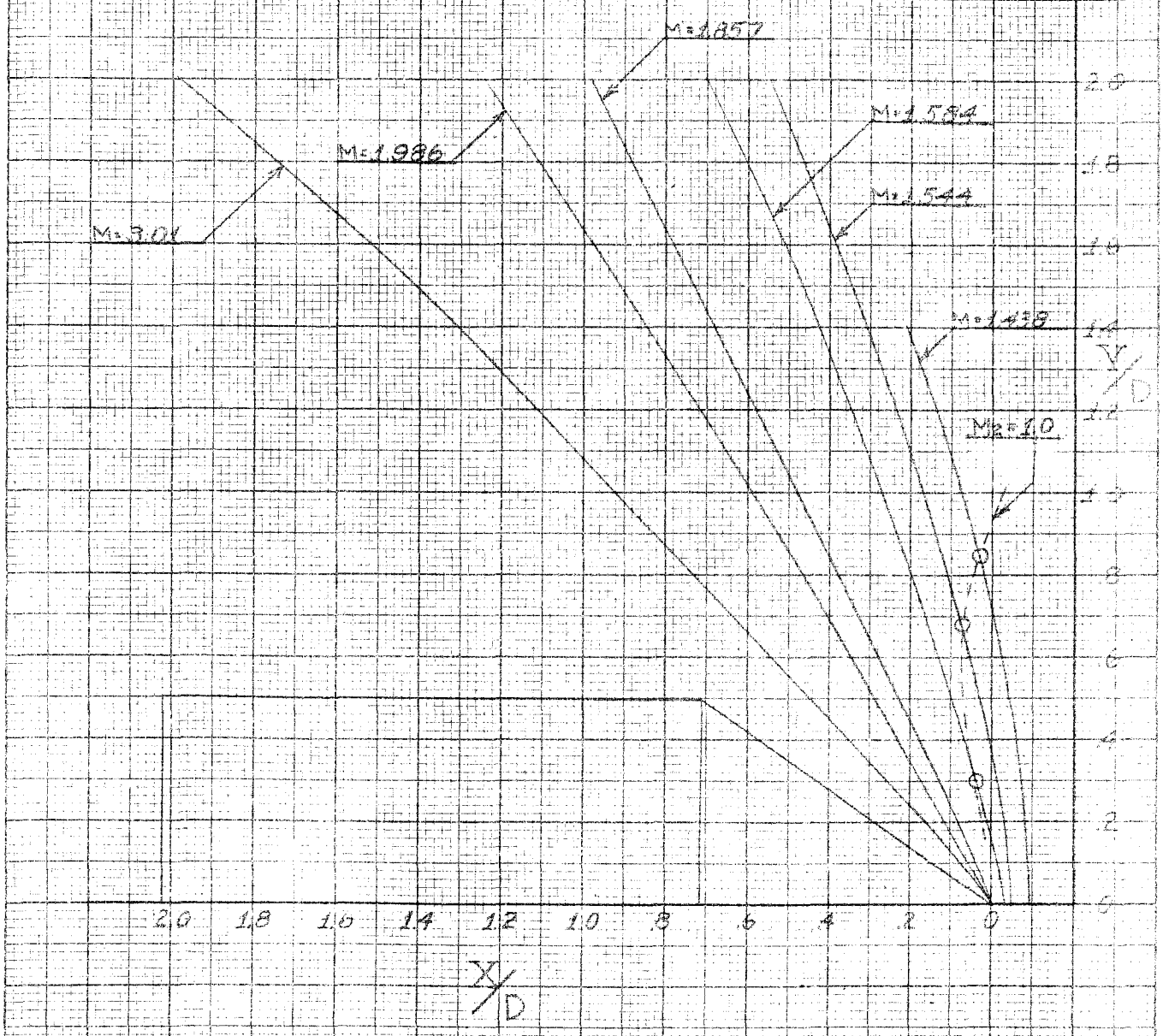

FIG. 24
$\alpha = 15°$
LOWER

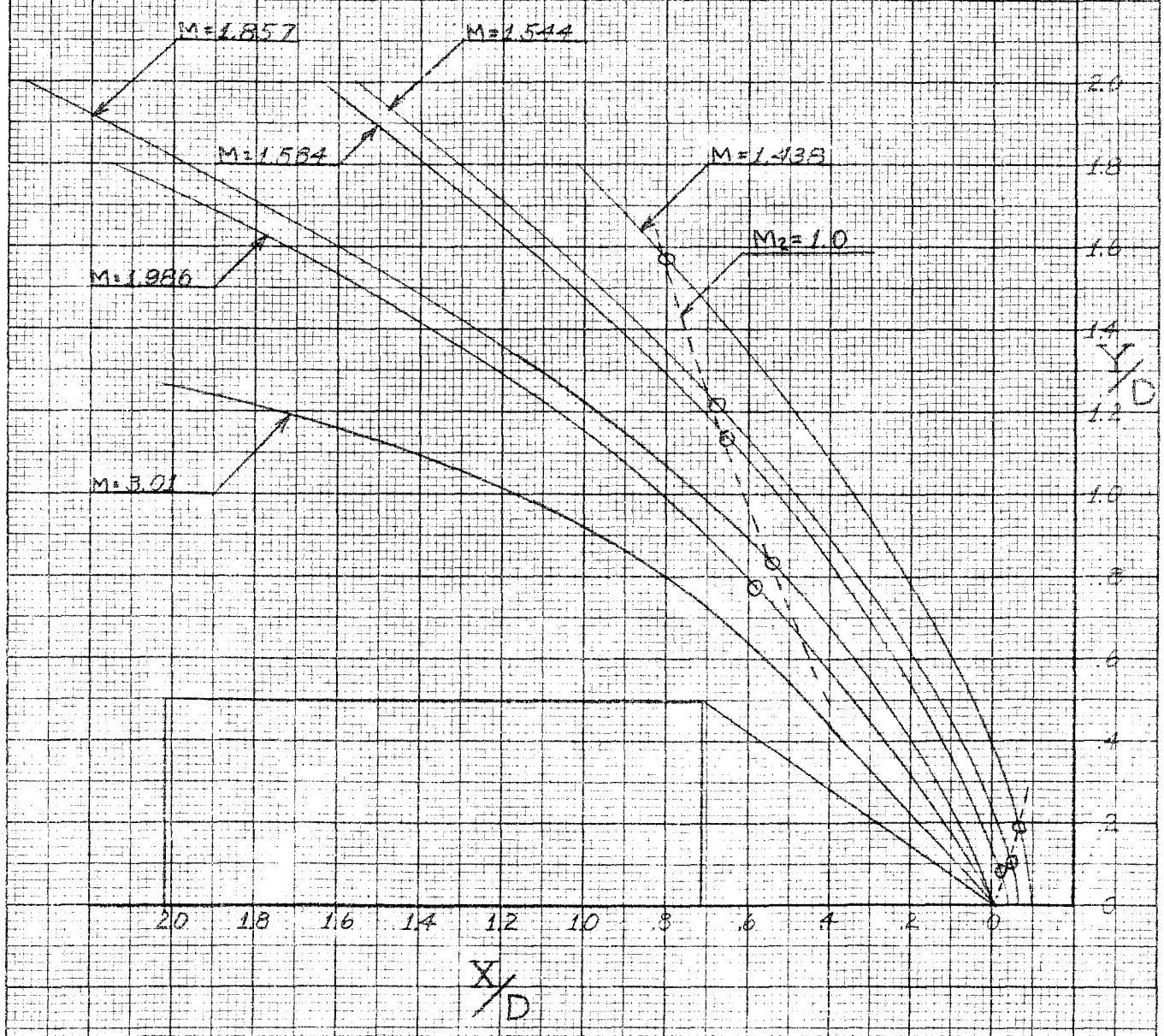

FIG. 25
$\alpha = 15°$
UPPER

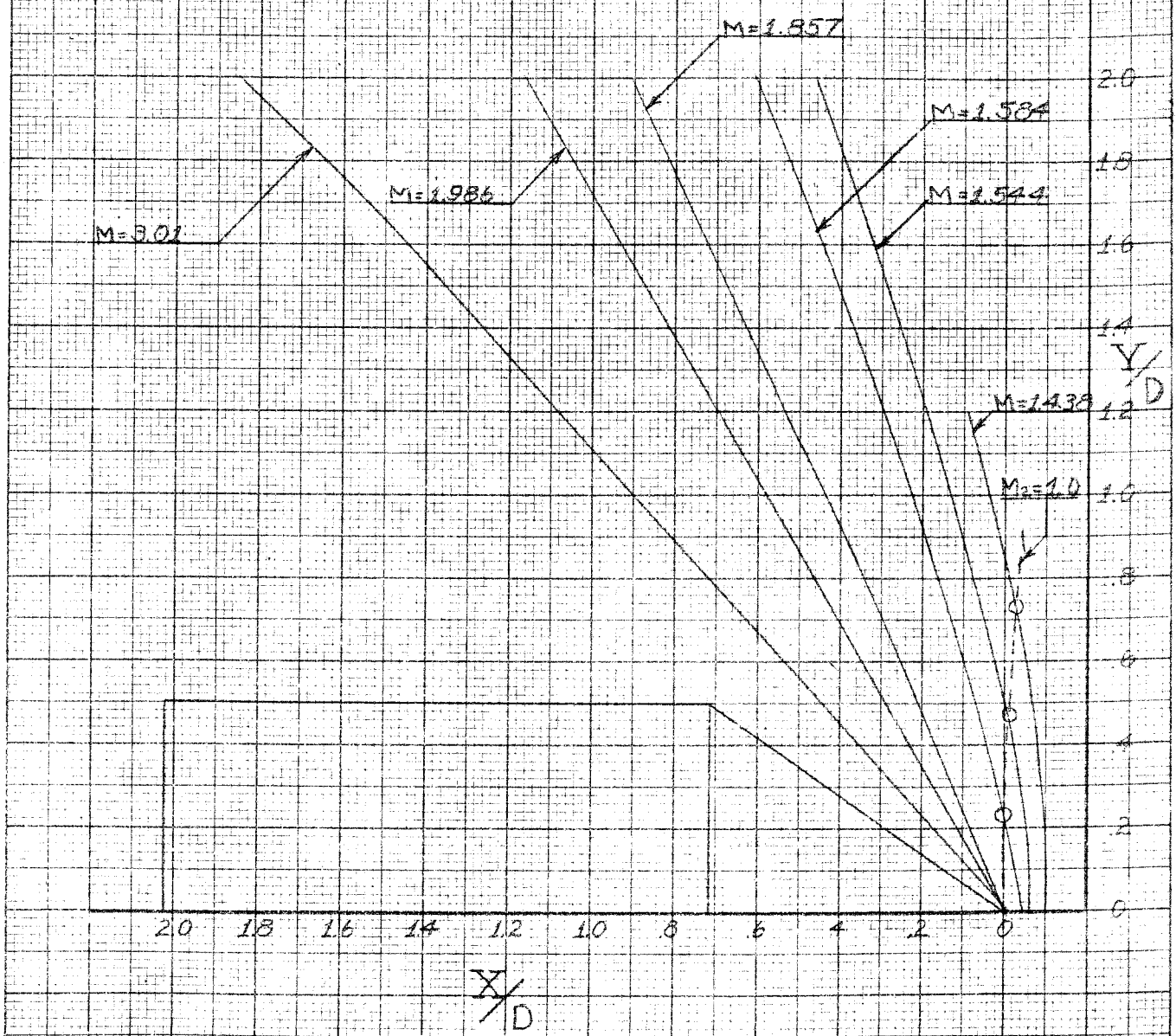

FIG. 26
MAXIMUM FLOW DEFLECTION
(TAYLOR-MACCOLL THEORY)

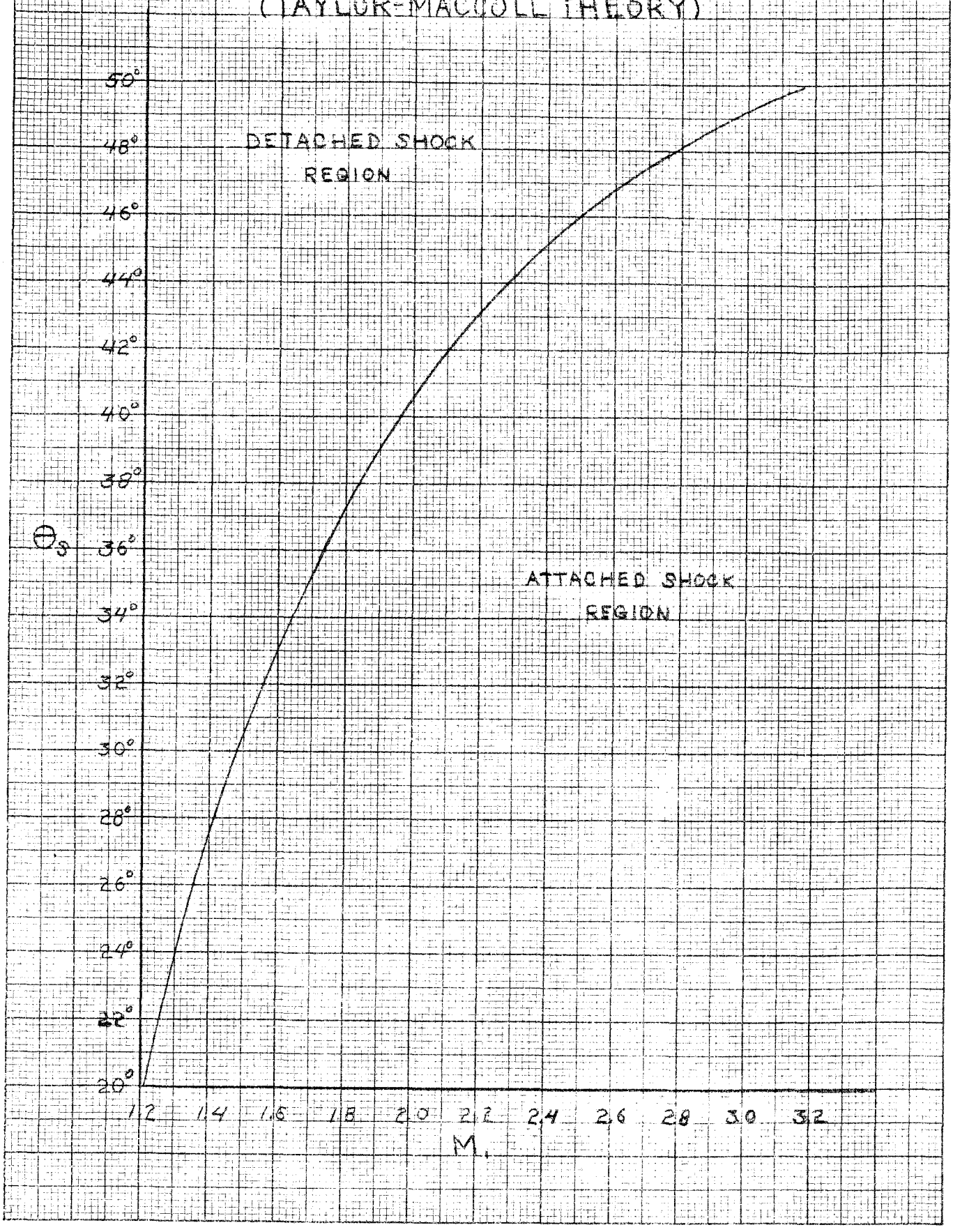

FIG. 27
SURFACE PRESSURE DISTRIBUTION
M = 1.584

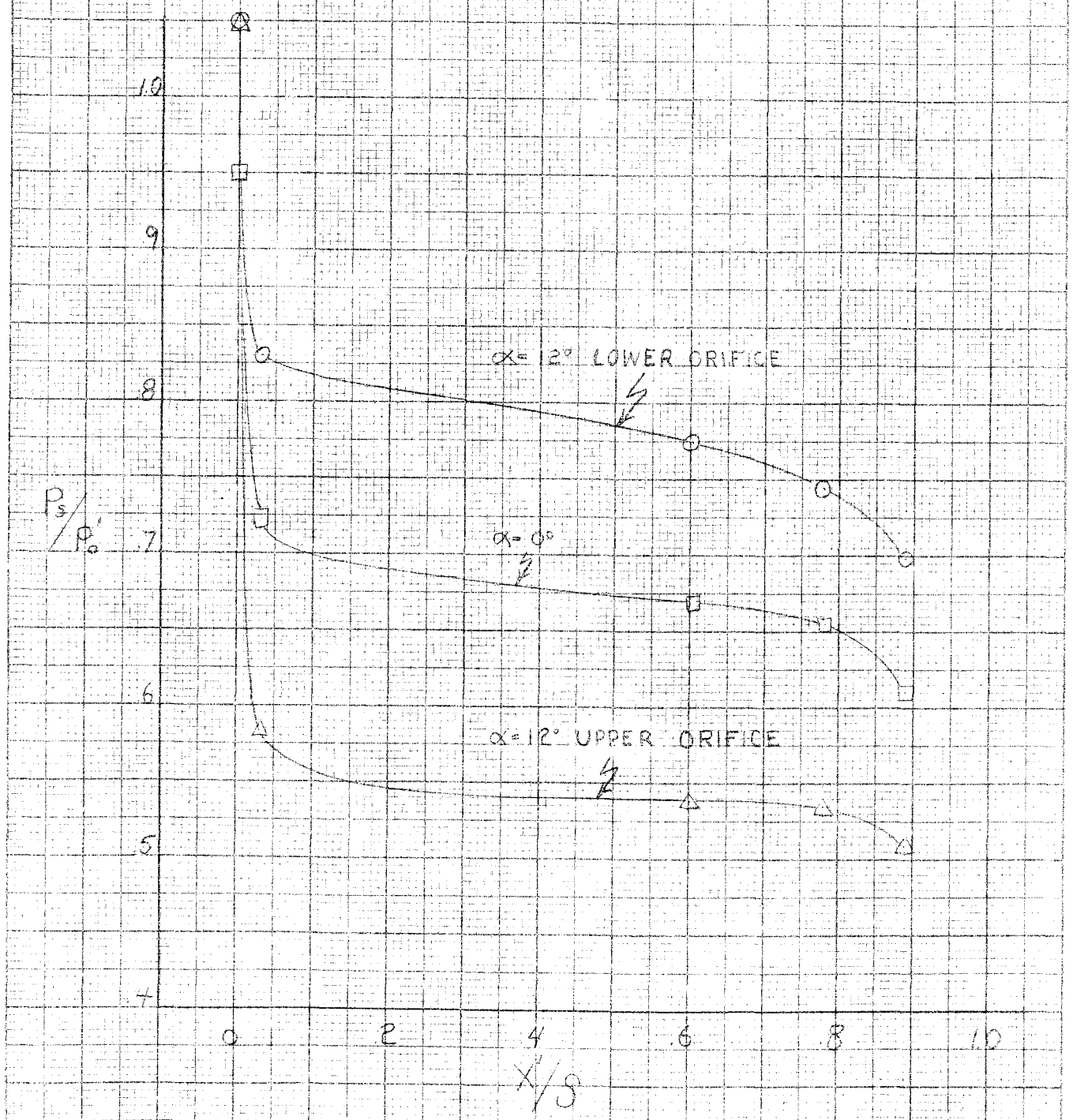

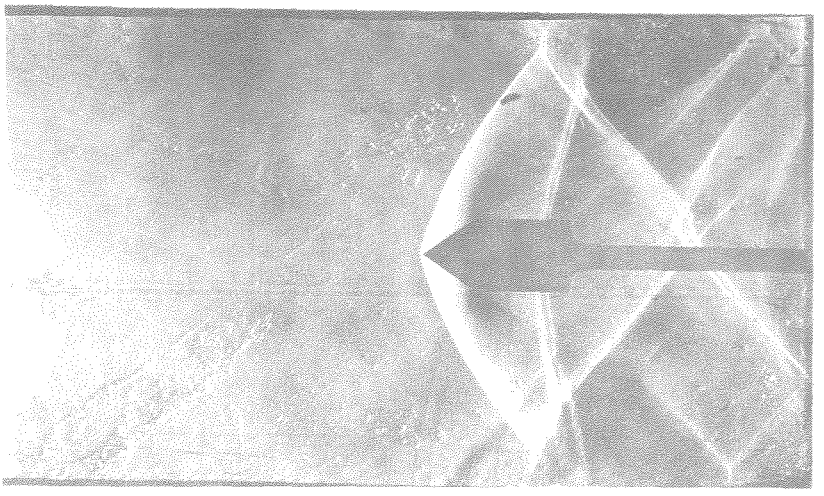

Fig. 28
M = 1.544
$\alpha = 0^{\circ}$

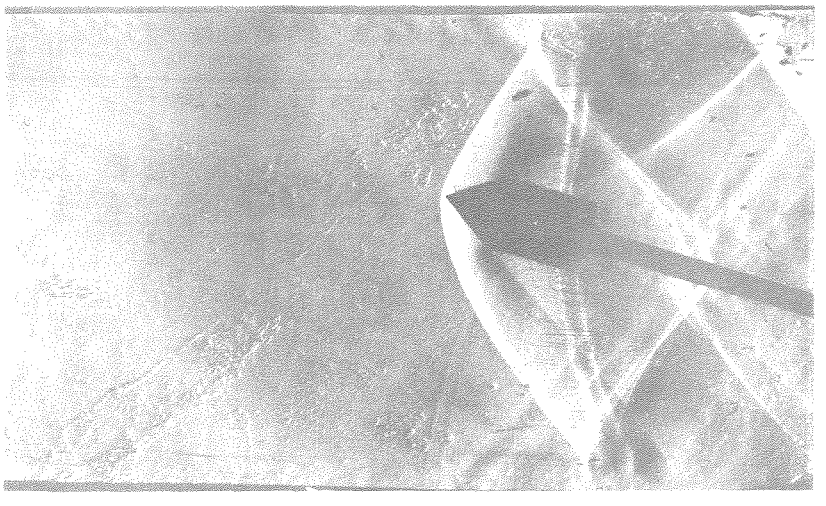

Fig. 29
M = 1.544
$\alpha = 15^{\circ}$

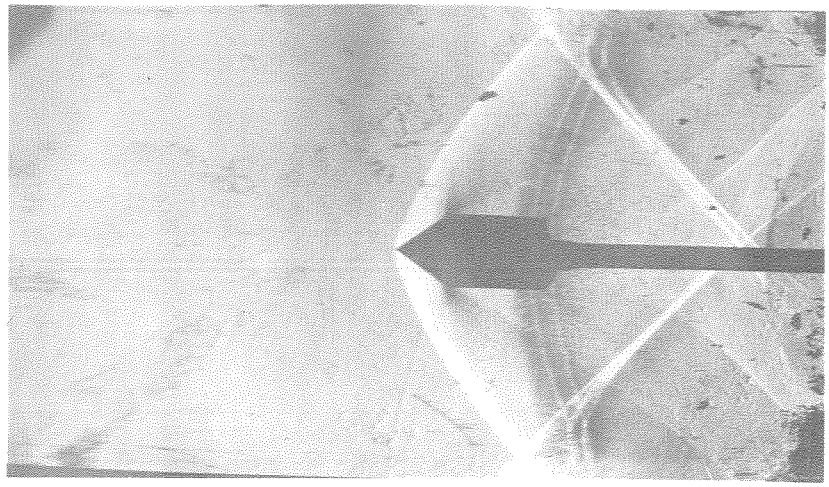

Fig. 30
$M = 1.584$
$\alpha = 0^{\circ}$

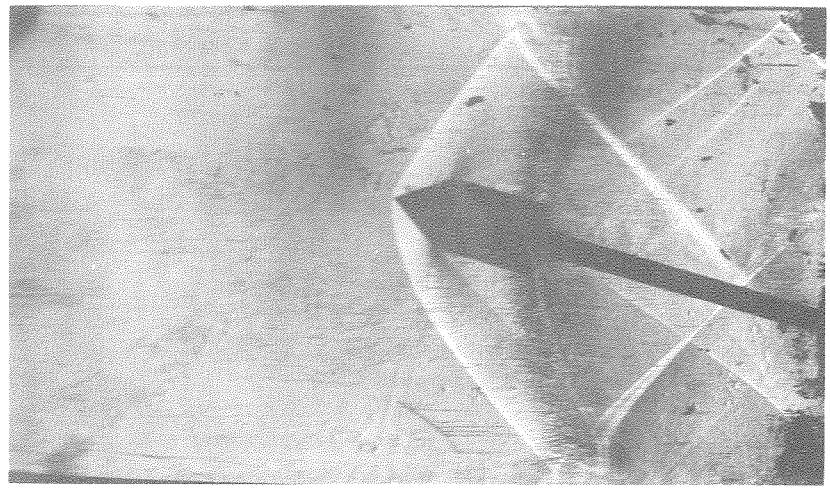

Fig. 31
$M = 1.584$
$\alpha = 15^{\circ}$

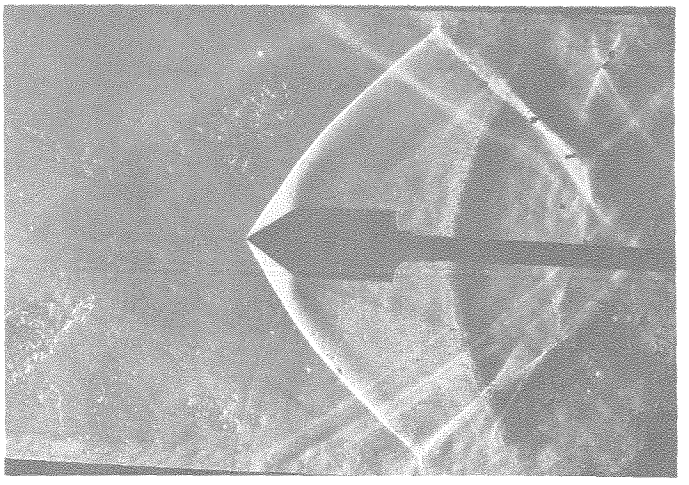

Fig. 32
M = 1.857
$\alpha = 0^{\circ}$

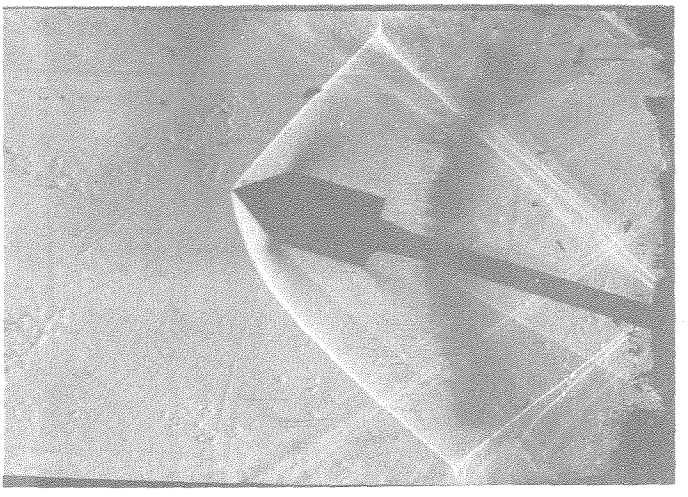

Fig. 33
M = 1.857
$\alpha = 15^{\circ}$